Review

Why Did Such Giant Stress Accumulate on the Joining of Four Tectonic Plates in Eastern Turkey? A Review

Lev V Eppelbaum *, Youri I Katz , Zvi Ben-Avraham

Posted Date: 17 August 2023

doi: 10.20944/preprints202308.1252.v1

Keywords: geodynamics; Turkish February 2023 earthquakes; rotating mantle structure; GPS; gravity; magnetic; and paleomagnetic data analysis

Review

Why Did Such Giant Stress Accumulate on the Joining of Four Tectonic Plates in Eastern Turkey? A Review

Eppelbaum L. V. [1,2,*], Katz Yu. I. [3] and Ben-Avraham Z. [1]

[1] Dept. of Geophysics, Faculty of Exact Sciences, Tel Aviv University, Ramat Aviv 6997801, Tel Aviv, Israel
[2] Azerbaijan State Oil and Industry University, 20 Azadlig Ave., Baku AZ1010, Azerbaijan
[3] Steinhardt Museum of Natural History & National Research Center, Faculty of Life Sciences, Tel Aviv University, Ramat Aviv 6997801, Tel Aviv, Israel
* Correspondence: levap@tauex.tau.ac.il

Abstract: The Easternmost Mediterranean is a junction zone between the largest Earth's lithospheric segments – Eurasian and African-Arabian, and a transition area from the ocean to the continent. The latest catastrophic earthquakes in eastern Turkey require their geodynamic understanding. The two most decisive events (with magnitude (M) = 7.8 and 7.7) were observed with an interval of 9 hours on February 06, 2023, followed by a whole series of about 10,000 significative aftershocks. These tragic events led to the death of more than 60 thousand people. The above values indicate the colossal tension created in the Earth's crust. The region where these strongest earthquakes occurred is a tectonically very complex junction zone of four tectonic plates: Eurasian, Arabian, African, and Anatolian. The joint movement of these plates (consisting, in turn, of tectonic elements of different ages) occurs at an average rate of 6–15 mm per year. However, after two marked powerful shocks and a series of aftershocks, some sectors of the Anatolian plate shifted to the southwest by more than 11 meters. What happened in eastern Turkey? The interaction of numerous factors complicates the tectonic–geodynamic characteristics of the region. Let us analyze what is the most influencing component. Our recent publications (Eppelbaum et al., 2020, 2021) indicated the presence of a giant, rotating quasi-ring structure below the Easternmost Mediterranean. The GPS vector map coinciding with the gravitational trend displays the counterclockwise rotation of this structure. A review of paleomagnetic data on the projection of the discovered structure into the Earth's surface confirms its mainly counterclockwise rotation. Analysis of the magnetic field ΔZ, geoid anomalies map, and seismic tomography data commonly prove the presence of this deep anomaly. The geodynamic and structural characteristics of the region and paleobiogeographic data are consistent with the proposed physical–geological model. A widespread analysis of tectonic, petrological, and mineralogical data implies a connection between the discovered deep structure and near-surface processes. An examination of numerous publications by different authors confirms the above phenomenon's existence. A crucial for understanding the nature of the considered seismic stress is its location near the expressed bend of the Mesozoic terrane belt, where the Arabian Plate is deeply intruded into the Alpine-Himalayan belt. Thus, the rotation of this giant deep structure may accumulate the stress effect and be one of the causative reasons for the last catastrophic geodynamic events in Eastern Turkey.

Keywords: geodynamics; Turkish February 2023 earthquakes; rotating mantle structure; GPS; gravity; magnetic; and paleomagnetic data analysis

 doi:10.20944/preprints202308.1252.v1

1. Introduction

Investigating the relationships between deep geodynamic events and surface (subsurface; the last term here can mean many tens of km) geological processes is one of the critical problems in solid earth sciences (Cloetingh and Willet, 2013; Cloetingh et al., 2018). A series of catastrophic seismic events in southeastern Turkey in February 2023 makes it necessary to consider the diverse tectonic-geodynamic and deep geophysical data to explain this natural phenomenon. This complex analysis procedure is necessary for developing regional monitoring sustainability of habitats and engineering infrastructures of this area – one of the most ancient in civilizational development. The anomalousness of the region is manifested in the tectonic-structural features of the mantle, lithosphere, and hydrosphere. A complex junction of oceanic and continental crust units is a distinguishing feature of the study region. The simultaneous development of collision processes (associated with the latitudinal zone of the Neotethys Ocean closure) and the manifestation of the initial stages of spreading of the Red Sea–Indian Ocean submeridional rift system further complicates the overall pattern.

The region where these strongest earthquakes occurred is a tectonically very complex junction zone of four tectonic plates: Eurasian, Arabian, African, and Anatolian (e.g., Tatar et al., 2004; Ben-Avraham et al., 2006; Faccenna et al., 2014; Uzel et al., 2015; Eppelbaum et al., 2018). Tectonically the considered area belongs to the Eastern Mediterranean, with its Cyprus-Levantine marine and Anatolian-Nubian-Arabian continental framing (Figure 1). The joint movement of these plates (consisting, in turn, of tectonic elements of different ages) occurs at an average rate of 6–15 mm per year (e.g., Rellinger et al., 2006). However, after two marked powerful shocks on 06.02.2023, the Anatolian plate shifted to the southwest by several meters (two tectonic segments – up to 11.2 and 11.5 m). These tragic events led to more than 60 thousand deaths, and many buildings and engineering constructions were destroyed. What is the main reason for such a powerful geodynamic event? We suggest that these catastrophic events were triggered mainly by the recently discovered (Eppelbaum et al., 2020, 2021) mantle quasi-circular counterclockwise rotating structure influencing many subsurface processes.

Preprints (www.preprints.org) | NOT PEER-REVIEWED | Posted: 17 August 2023 doi:10.20944/preprints202308.1252.v1

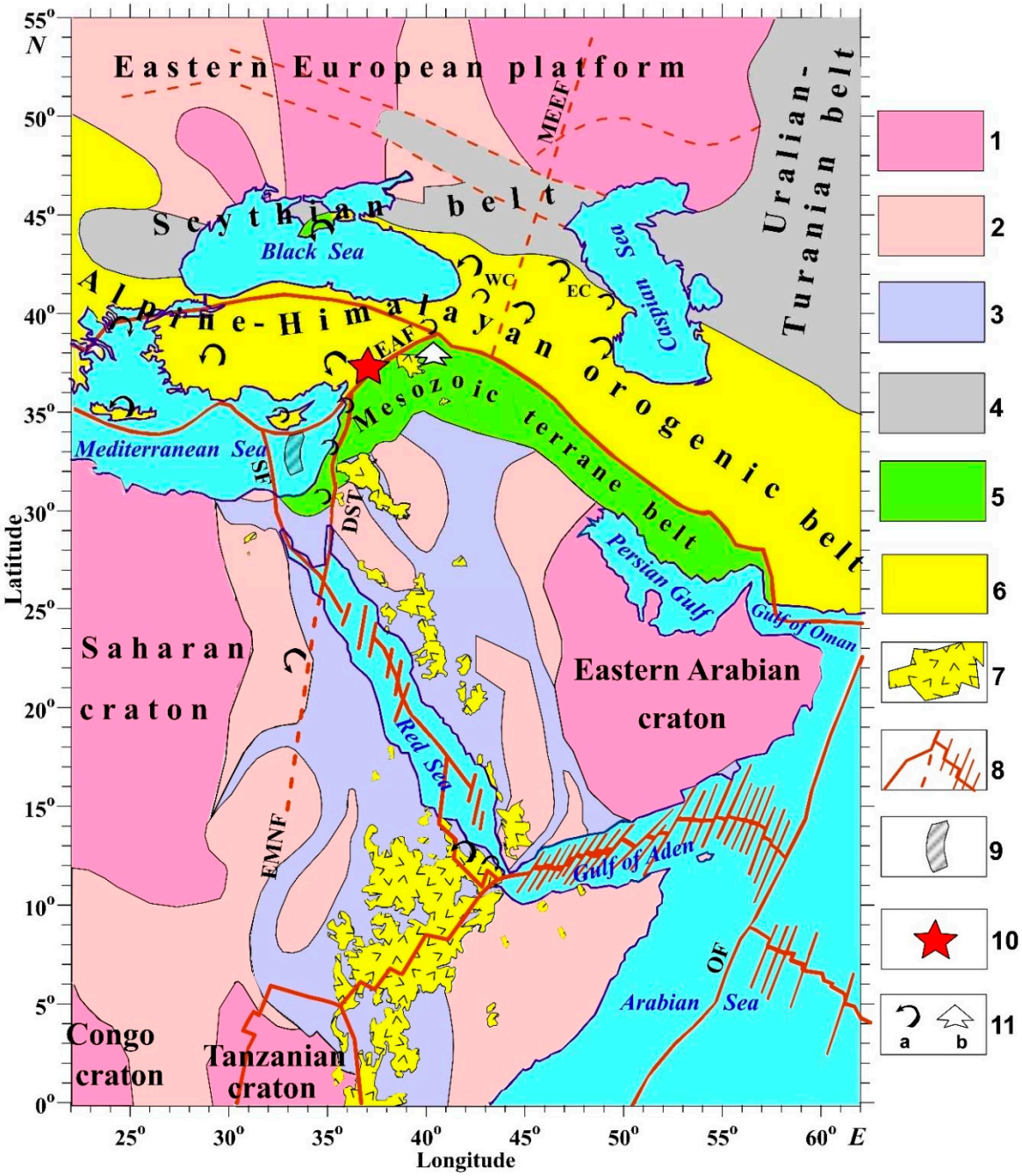

Figure 1. The tectonic-geodynamic scheme of the region under study (modified after Eppelbaum et al., 2021). (1) Archean cratons, (2-4) folded belts: (2) Paleo-Middleproterozoic, (3) Neoproterozoic, (4) Late Paleozoic (Herzynian), (5) Mesozoic terrane belt (MTB), (6) Alpine-Himalayan orogenic belt, (7) Cenozoic traps of the African-Arabian rift belt, (8) main fault systems, (9) contour of the Kiama paleomagnetic hyperzone of inverse polarity (after Eppelbaum et al., 2014; Eppelbaum and Katz, 2015), (10) high magnitude seismogenic zone in Eastern Turkey (February 06, 2023), (11) **a**: rotational geodynamic elements derived from paleomagnetic data, **b**: distal part of the MTB. SF, Sinai Fault, DST, Dead Sea Transform, MEEF, Main Eastern European Fault, EMNB, Eastern Mediterranean Nubian Belt, OF, Owen Fault, WC, Western Caucasus, EC, Eastern Caucasus, EAF, Eastern Anatolian Fault.

 doi:10.20944/preprints202308.1252.v1

2. Brief Geological-Geophysical Background

This paper presents an integrated analysis of the North Africa–West Asia region, where giant tectonic plates and several comparatively small tectonic units interact (Faccenna et al., 2014). This region includes numerous active faults and interacting tectonic belts, a complex outline of continental and oceanic crust of different ages, high-intense geodynamic activity, and several high-amplitude gravitational anomalies. Besides this, this region is also characterized by significant seismic velocity deviations observed at great depths that testify to the non-conventional structure of the upper and lower mantle. In this region, zones of the final subduction phases and initial rifting (spreading) stages are comparatively close in location (Faccenna et al.; 2003; Muttoni et al., 2003; Reilinger et al., 2006; Stampfli et al., 2013; Eppelbaum et al., 2018; Rolland et al., 2020). The geological–geophysical instability of this region, located in the junction zone between East Gondwana and Eurasia, is determined by geodynamic intensity – both collisional and rifting types (Figure 1). Here, different fold belts and cratons have developed, and diverse geophysical-geodynamical processes are manifested (Stern and Johnson, 2010; Stampfli et al., 2013; Faccenna et al., 2014; Jolivet et al., 2016).

The region is at the boundary planetary zone between Eurasia's two largest plate-tectonic zones and Central Gondwana. The Eurasian segment includes the East European platform, the Late Paleozoic Scythian-Turanian belt, and the Alpine-Himalayan orogenic belt dissected by a fault with residual basins of the Paratethys basin – the Black and Caspian Seas (Figure 1). The southern (Central Gondwana) plate-tectonic segment is composed of the Early Precambrian cratons of the western (Nubian) zone – Saharan, Congo, and Tanzanian and the East Arabian craton (EAC). Between the Nubian zone and the EAC, a powerful submeridional Neoproterozoic fold-metamorphic belt is developed (Eppelbaum et al., 2018). Diagonally this Precambrian structure is dissected by faults of the newest Red Sea rift system.

The youngest mobile belt of the Arabian zone is pre-Cenozoic. It is a fold-block arc of the Mesozoic terrane belt (MTB), deeply advanced to the north into the zone of the Alpine-Himalayan orogenic belt. Its distal part is shown with the corresponding sign (Figure 1). It is significant that in the zone of this joint, the width of the Alpine belt of the Pontic-Caucasian zone is reduced to a minimum – about 500 km. Furthermore, to the west, from the Cyprus arc to Eastern Crimea, the width of the Alpine belt exceeds 1200 km.

The analysis of the structural-tectonic position of the Turkish seismic phenomenon is well complemented by the data of supra-regional geodynamic zoning of the transition zone between Eurasia and Central Gondwana (Figure 2).

Several heterogeneous structures were identified in an extensive zone from 0 to 55° of northern latitudes, at the intersection of which an anomalous seismic zone is located. First, this is the critical parallel of 35°, within which the most intense shifts occur due to the Earth's figure meridian skew (Véronnet, 1912). Near this parallel, the junction boundary of Eurasian, Arabian, Anatolian, Sinai, and Nubian lithospheric plates passes (Eppelbaum et al., 2021). According to the same work, in the indicated space of the planetary joint, the data on satellite geodesy differ most sharply with the development of an intensive turn of tectonic blocks to the west and southwest in a counterclockwise direction (Barka and Reilinger, 1997; McClusky et al., 2000; Tatar et al., 2004).

However, the most crucial feature of the geodynamics of the region, the most essential for understanding the seismic phenomenon under consideration, is the discovery and mapping of an extensive sub-oval structure of the deep mantle, rotating in a counterclockwise direction (Eppelbaum et al., 2020, 2021). The axial part of this structure stretches from SSE to NW, as can be seen from the nature of the location of the isolines of the structure itself (Figure 2). Cyprus is in the center of this mantle structure projection, and the zone of anomalous seismicity in Eastern Turkey is in the zone of transition from the arch of the uplift ENE; this fact is essential for further analysis.

Preprints (www.preprints.org) | NOT PEER-REVIEWED | Posted: 17 August 2023 doi:10.20944/preprints202308.1252.v1

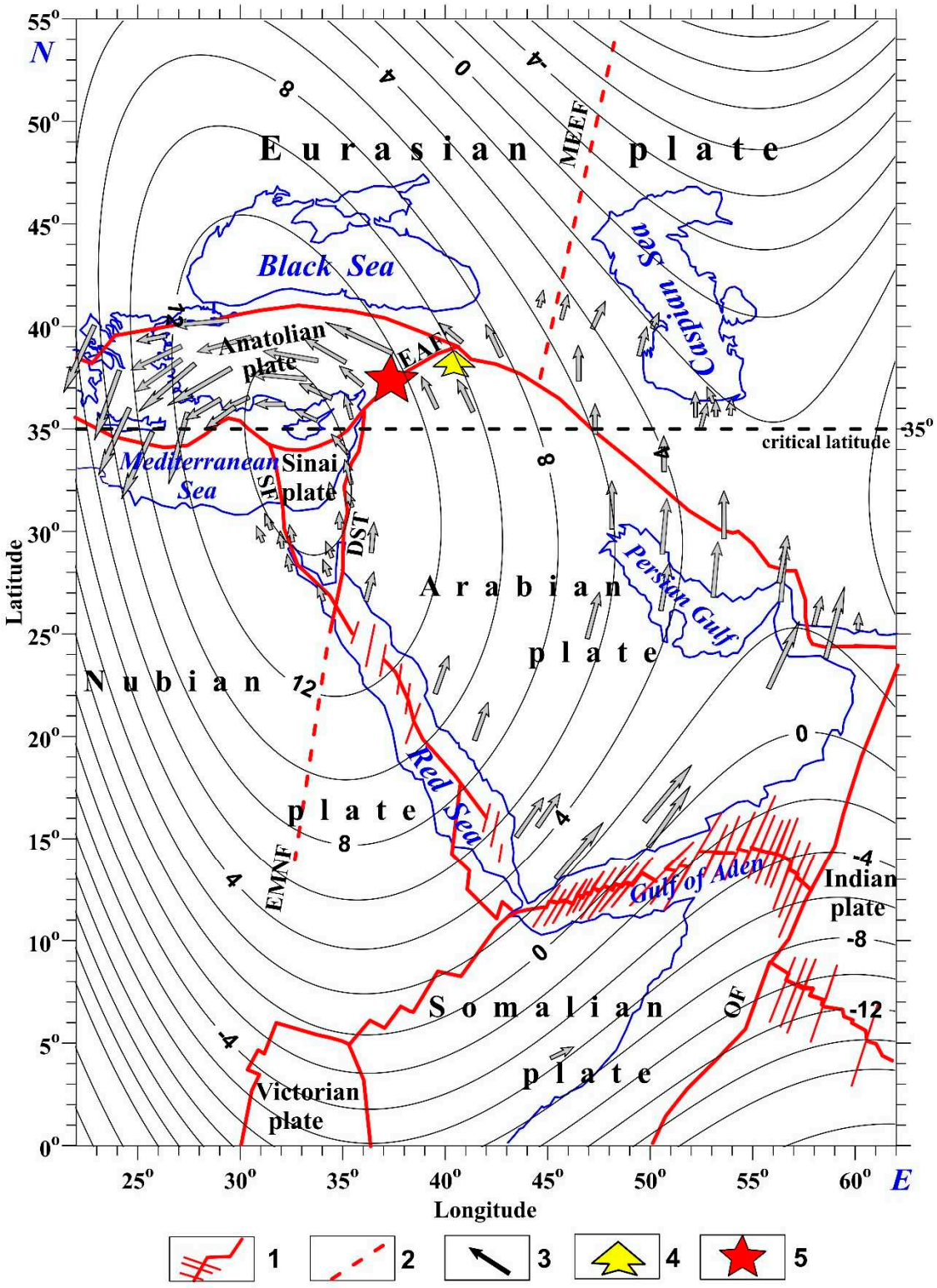

Figure 2. Integrated scheme of geodynamic indicators distribution of the region under study (overlaid by the residual gravity anomalies) (after Eppelbaum et al. (2021), modified and supplemented). (1) main interplate faults, (2) main intraplate faults, (3) vectors of the GPS monitoring (after Reilinger et al. (2006)), (4) distal part of the Mesozoic terrane belt, (5) high magnitude seismogenic zone in Eastern Turkey (February 06-07, 2023).

 doi:10.20944/preprints202308.1252.v1

3. Applied Geophysical-Geological Methods

The applied multidisciplinary set of geophysical and geological methods is presented below.

3.1. Satellite-derived gravity field analysis

Analysis of satellite gravimetric data is an effective tool for regional tectonic–geodynamic zonation, including comprehensive tectonic–structural interpretation, data transformation, and segmentation (Boschi et al., 2010; Eppelbaum and Katz, 2012, 2015, 2017, 2020; Kaban et al., 2016; Eppelbaum et al., 2018). The satellite-derived gravimetric data for this study were obtained from the World Gravity DB as retracked from the Geosat and ERS missions (e.g., Sandwell and Smith, 2009). Eppelbaum and Katz (2017) have exposed that to an examination of the deep structure of large regions (several million km^2 or more), satellite gravity data retracked to the Earth's surface can be employed without any reductions. Eppelbaum et al. (2021) have investigated a satellite gravimetric dataset for the region of 0°–55° N and 22°–62° W. To recover the nature of anomalous sources, we used polynomial approximation, a powerful instrument for solving various problems in applied sciences (e.g., Barbeau, 2003).

Processing the 'Big Data' satellite gravimetric dataset (more than 9.5×10^6 measurements were used) removes abundant random elements. The anomalous gravity trend obtained with the polynomial cubic surface approximation is commonly like results taken from distance filtering and nonlinear methods. The main trend in all the above-mentioned gravity maps displays a deep oval (quasi-ring) anomaly superficially reflecting a deep target creating this anomaly (Figure 2). It is the standard procedure to analyze quantitatively transformed potential (magnetic, gravity, thermal, etc.) field anomalies (e.g., Khesin et al., 1996; Telford et al., 1991). The residual gravitational anomaly was interpreted using methods (improved tangent, characteristic point, and areal) especially developed to analyze potential geophysical anomalies when the level of the normal field is unknown (Eppelbaum and Khesin, 2012). Application of these methods indicated that the upper edge of the giant deep quasi-ring structure occurs at 1650– 1700 km. Thus, the anomalous source occurs in the lower mantle of the Earth.

3.2. Land/marine gravity field analysis

The global geological structure geodynamic analysis testifies that arched zones are mostly unstable segments (especially in the case of rotation) (Aleinikov et al., 2001). An intense trend of the Bouguer gravity anomalies sharply outlines the Red Sea spreading zone (Makris et al., 1991) (Figure 3c). It coincides with the long axis of the satellite-derived residual gravity data (Figure 3a). At the same time, the high-amplitude Cyprus gravity anomaly (Gass and Masson-Smith, 1963) (Figure 3b) exactly coincides with the center of the residual gravity anomaly. The map presented in Figure 3c shows that in the axial zone of the Red Sea rift, the Bouguer anomalies reach almost +100 mGals, along the long axis of the recognized structure. Figure 3c is consistent with other geological–geophysical data, indicating asymmetry of the structure and movements of both sides of the neotectonic rifting zone (Bosworth et al., 2005) in the Red Sea region. Thus, there was a good agreement between the three types of independently observed gravimetric data.

Analysis of the Bouguer gravity anomalies in the western and eastern frames of the Red Sea crosscutting the system of igneous and metamorphic complexes shows regional asymmetry in the distribution of the gravity field characteristics (see Figure 3c). In the west, within the Nubian Plate, the Bouguer anomalies are near stable platform values: ±50 mGals. In sharp contrast to these data, on the eastern coast, corresponding to the Arabian Plate (where extended fields of the Late Cenozoic dikes and effusive traps have developed), the Bouguer anomalies, which are linearly elongated parallel to the Red Sea coast, are characterized by pronounced negative values, which is typical for activated platforms.

Preprints (www.preprints.org) | NOT PEER-REVIEWED | Posted: 17 August 2023 doi:10.20944/preprints202308.1252.v1

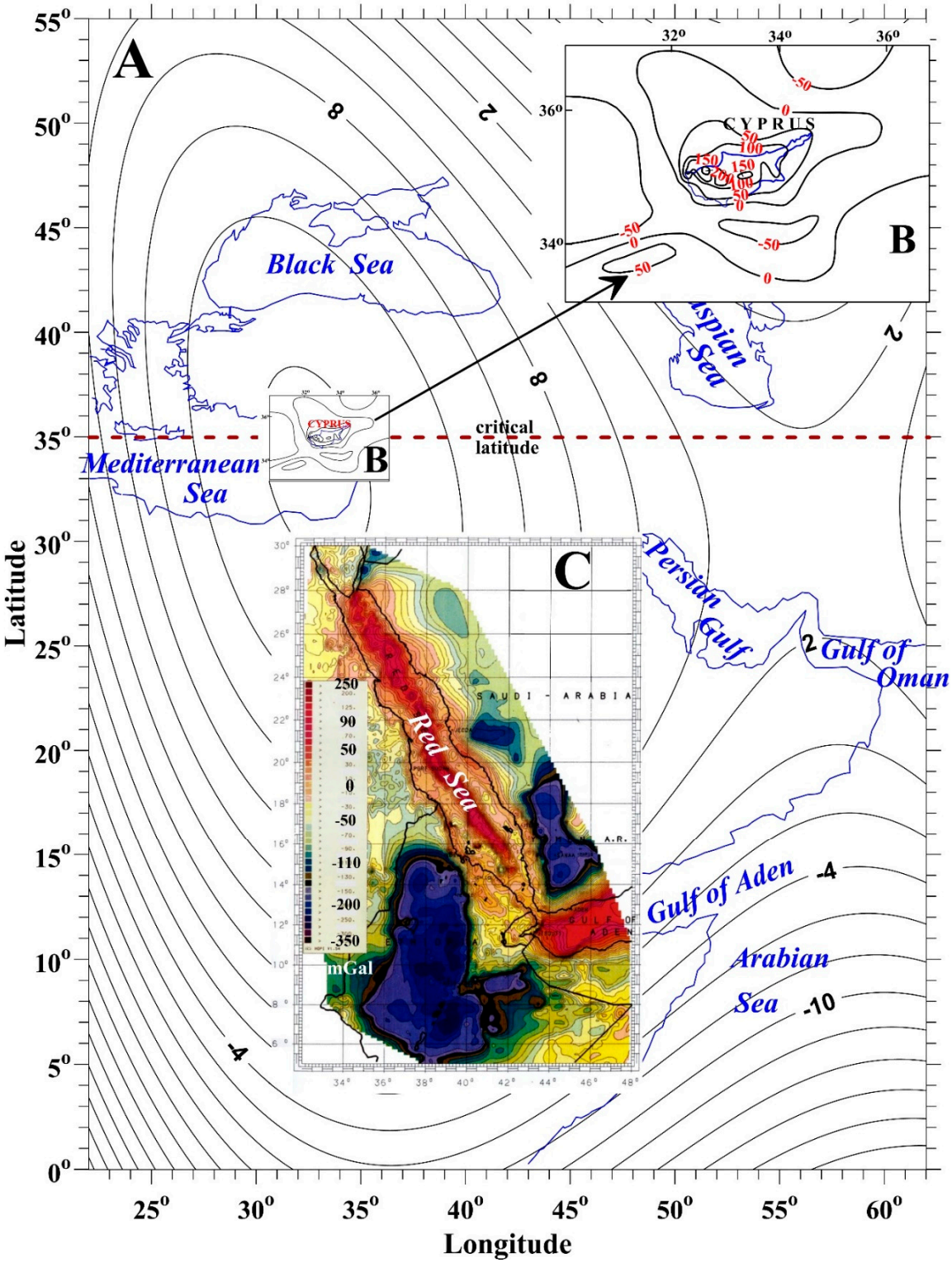

Figure 3. Comparison of gravitational anomalies (modified after Eppelbaum et al., 2021): (a) Residual satellite-derived gravity anomaly, (b) Cyprus isostatic gravitational anomaly (land/sea) (after Gass and Masson-Smith, 1963); (c) Bouguer anomalies observed in the Red Sea and adjacent areas (sea/land) (after Makris et al., 1991). The dashed line indicates 35° critical latitude of the Earth.

Preprints (www.preprints.org) | NOT PEER-REVIEWED | Posted: 17 August 2023 doi:10.20944/preprints202308.1252.v1

The developed satellite-derived gravity gradient map (Figure 4) shows that the seismicity anomalous zone is confined not to the axial zone of the deep mantle structure but to its periphery.

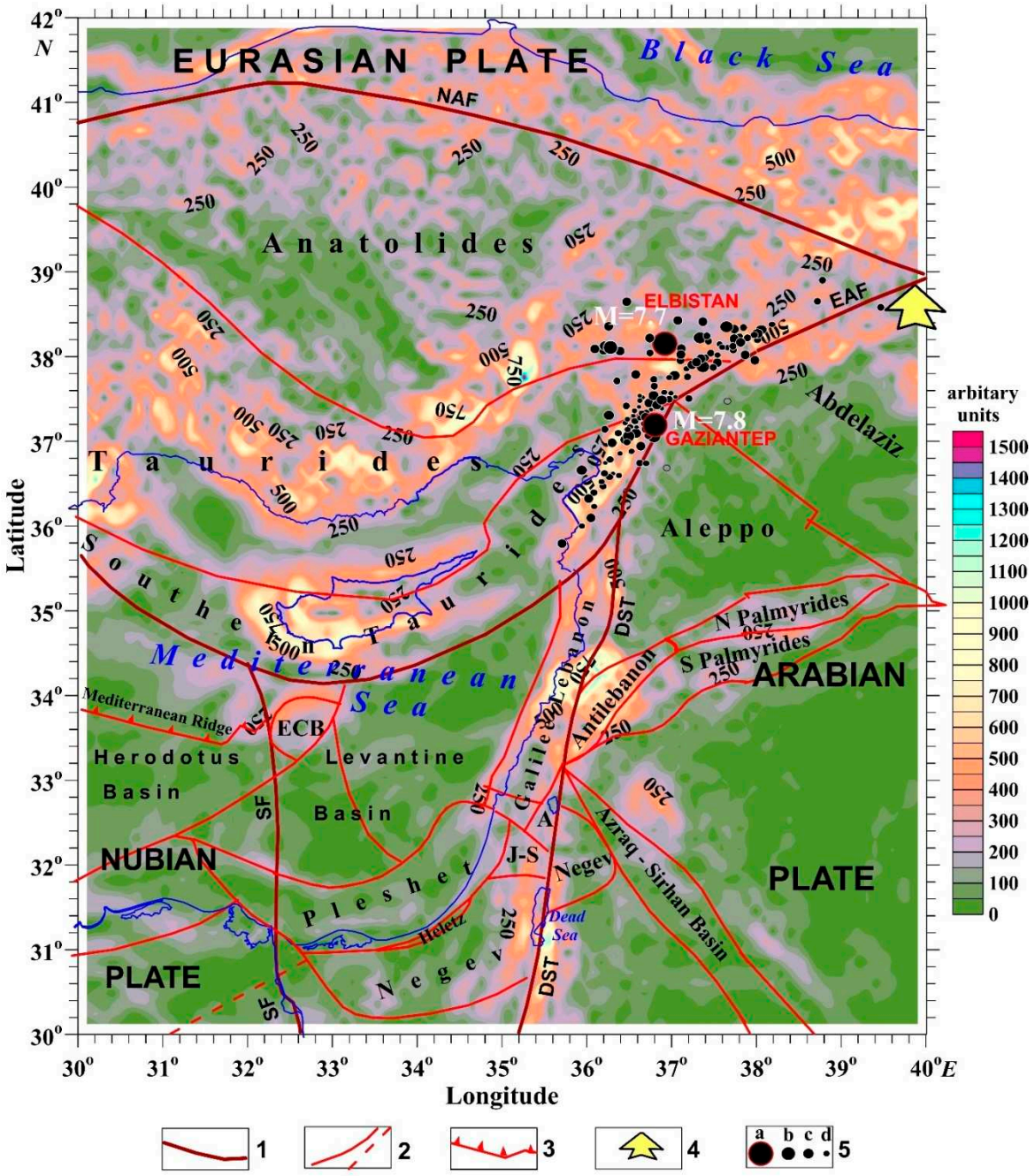

Figure 4. Satellite-derived gravity gradient map with the main tectonic elements and seismological features in eastern Turkey. (1) main fault systems, (2) interplate and intraplate faults, (3) Mediterranean Ridge, (4) distal part of the Mesozoic terrane belt, (5) Magnitudes on earthquakes registered 06.02.2023 in eastern Turkey till 13.15 UTC: a: > 7.5, b ≥ 6.0, c: ≥ 4, d: ≤ 4 (magnitudes after Garini and Gazeras, 2023 and SCEM DB). ECB, Eratosthenes Continental Block, DST, Dead Sea Transform, SF, Sinai Fault, J-S, Judea-Samaria, A, Antilebanon, NAF, Northern Anatolian Fault, EAF, Eastern Anatolian Fault.

 doi:10.20944/preprints202308.1252.v1

In other words, the gradient gravity map showed the deviation of the seismic zones in the direction to the west of the distal bulge of the Arabian lithospheric plate, i.e., counterclockwise. This follows from the analysis of the gradient data: the Arabian, Sinai, Nubian, and central parts of the Anatolian plate have minimal gradient values, up to 300 units, and in the zones of plate junction, they reach a value of 1000 unit, which can be seen in the junction zone of the regional faults DST, EAF, and the Cyprian arc. This additional element of the crust's stressed state is not decisive for determining the genesis of the considered seismic phenomenon but, undoubtedly, can be used if new geological and geophysical data are involved, which will be shown below. The constructed map (Figure 4) precisely agrees with the map of the earthquake distribution (altogether 178 events) registered on 06.02.2023, till 13.15 UTC (Garini and Gazeras, 2023).

3.3. GPS vectors behavior

The GPS pattern was reconstructed by Reilinger et al. (2006) (mainly) and Doubre et al. (2017) (partially) unambiguously indicates the clearly visible counterclockwise rotation in the region under study (Figure 1) (Eppelbaum et al., 2020).

3.4. Map of geoid isolines evaluation

It is known that the geoid map reflects combined effects from the Earth's crust, mantle, and core (Richards and Hager, 1984; Ricard et al., 1989; Mao and Zhong, 2021). The generalized geoid anomalies for the study region (based on the EMG2008 data) and their comparison with the GPS pattern are shown in (Eppelbaum et al., 2021). The geoid isolines behavior presents the huge quasi-circular anomaly elevations reflecting the deep quasi-circular arch structure and lows – his periclinal parts. Geodynamically, this map agrees well with the GPS data behavior and the residual gravitational field (Eppelbaum et al., 2021). The geoid anomalies also show a correlation with the primary regional tectonic units.

3.5. Paleomagnetic data generalization

It is well-known that paleomagnetic data are the main indicators of tectonic block rotation (Kissel and Laj, 1988; McElhinny, 1989; Tauxe, 2002). The study of the geodynamics of the central part of the projection of the deep anomalous ring structure (including the western margin of the Neoproterozoic fold belt, the structural zones of the Eastern Taurides, southern and northern margins of the Mesozoic terrane belt, Cyprus arc, Crete Island, Aegean Sea, and Western Carpathians) indicates that the tectonic block rotation is predominantly counterclockwise (Figure 1) (Khramov, 1984; Nur et al., 1989; Le Pichon et al., 1995; Duermeijer et al., 1998; Kissel et al., 2003; Marchev et al., 2004; Tatar et al., 2004; Borradaile et al., 2010; Henry et al., 2010; Eppelbaum and Katz, 2015; Lotfi, 2015; Gürer et al., 2017; Çabuk and Cengiz, 2021; Lazos et al., 2022). In the Western Caucasus, relating to the peripheral part of the projection of the deep structure, the prevailing counterclockwise block rotation is observed (Bazhenov and Burtman, 2002; Hisarli, 2011; Rolland, 2017). In contrast, the Eastern Caucasus zones of uplifts and troughs located outside the contour of the mantle structure projection, the crustal block clockwise rotation has been recognized (Khramov, 1984; Bazhenov and Burtman, 2002; Khalafly, 2006; Hisarli, 2011; Rolland, 2017) (Figure 1).

Studies of paleomagnetic data in the peripheral parts of the deep structure projection show, as a whole, geodynamic instability (Eppelbaum et al., 2021). However, paleomagnetic rotations in the central part of the mantle structure projection are mainly counterclockwise (Figure 1) and agree with the counterclockwise GPS vector behavior, the residual gravity field isolines (Figure 2), and geoid anomalies (Eppelbaum et al., 2021).

In detail, let us consider three typical examples of tectonic block counterclockwise paleomagnetic rotations. For performing optimal paleomagnetic mapping, a suitable classification is necessary. The development of Jalal, Sogdiana, Gissar, Tuarkyr, and Khorezm paleomagnetic arrangement is presented in (Molostovsky et al., 2007; Pechersky et al., 2010).

Preprints (www.preprints.org) | NOT PEER-REVIEWED | Posted: 17 August 2023 doi:10.20944/preprints202308.1252.v1

3.5.1. Cyprus area

Morris et al. (2002) have shown that the ophiolite massifs of Troodos (Cyprus) and Baer-Bassit (Syria) underwent substantial counterclockwise rotation. Paleomagnetic reconstructions enabled to compile the geodynamic diagrams demonstrating the counterclockwise rotation of the Cyprus structure from the Cretaceous to the Late Cenozoic (Figure 5).

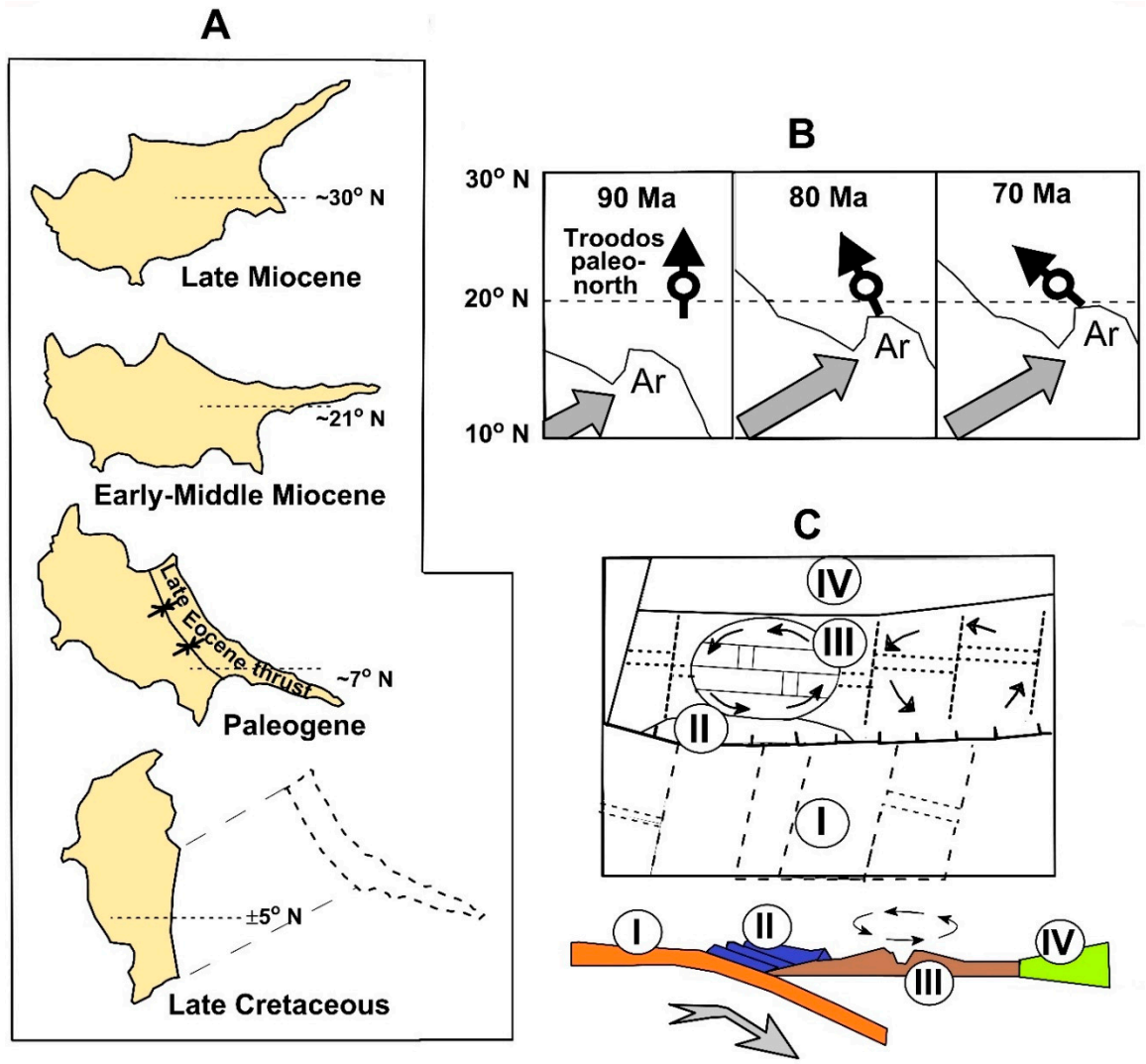

Figure 5. Cyprus geodynamic schemes of the counterclockwise rotation (Cretaceous–Late Cenozoic) (modified after Eppelbaum et al., 2021): (A) counterclockwise rotation of Cyprus from Late Cretaceous to Late Miocene (based on the paleomagnetic data (Borradaile et al., 2010)), (B) change in the relative position of Cyprus and the African–Arabian Plate of Gondwana paleocontinent in the Late Cretaceous (based on the paleomagnetic data (Morris et al., 2002)), (c) Cyprus paleostructures paleogeodynamic reconstruction of within the Late Cretaceous Tethys Paleo Ocean and its frame (after Hall et al., 2005). I, subducting oceanic plate of the Neotethys southern side; II, ophiolite complex of the Early Mesozoic crust of Mammonia basin; III, spreading zone of the Late Cretaceous part of the middle Troodos ridge; IV, terrane zone of the Aegean–Anatolian belt with the continental crust.

 doi:10.20944/preprints202308.1252.v1

3.5.2. Makhtesh Ramon area (Southern Israel)

The Makhtesh Ramon terrane (Southern Israel) is the extreme southwestern part of the MTB, collisional articulated with the Arabian-Nubian part of Gondwana (Eppelbaum and Katz, 2015). This fact explains the high complexity of the Ramon subterrane structure, which contains various geological-geophysical tectonic-structural elements. Paleogeodynamically development of this subterrane was formed during the pre-collisional, collisional, and post-collision stages.

The subterrane (Figure 6) has a wedge-shaped outline, the narrowed part of which is in the southwest and extends to the northeast. The paleomagnetic scheme (Figure 6A) and the diagram of the historical and geodynamic reconstructions (Figure 6B) conventionally depict not all subterrane but the outline of its submerged part corresponding to the erosion-tectonic depression, enclosing the Mesozoic outcrops (Lower Cretaceous, Jurassic and Triassic) and Late Cenozoic (Sneh et al., 1998). These rocks are permeated by a variety of Mesozoic traps, whose radiometric ages range from 165.7 to 93.8 Ma (Lang and Steinitz, 1989) and contain the outcrops of the ophiolite plates of the Saharonim basalts (Eppelbaum and Katz, 2015), the radiometric age of which is refined within 205 and 207 Ma (Segev, 2000). They correspond in age to the Illawarra-2 superzone, confirming the paleomagnetic studies' data (Baer et al., 1995), determining their normal polarity.

In Makhtesh Ramon, we used the analysis of the discontinuities and hypsometry of the plateau framing the canyon itself and outlines of the erosional canyon. The latter is essential because the boomerang-like canyon outlines with a deviation of the southwestern end to the east, and northeast – to the west, indicating the counterclockwise rotation of this subterrane. At the same time, the highest hypsometric marks exceeding 1000 m are in a narrow zone corresponding to the center rotation of the tectonic block. The cirrus nature of tectonic ruptures, spherical in places with prominent shear-slip elements, confirms the regional nature of the rotation of the structure, mainly in the counterclockwise direction. To analyze the evolution of movements of the Ramon subterrane (Figure 6B) was used to examine the movement of the radiometrically dated dikes and chains of the effusive rocks displaced from the primary latitudinal orientation. The performed studies showed that during almost the entire Jurassic-Middle Cretaceous stage, the area experienced a movement from the Neotethys Ocean southern side to the southwest with a concomitant counterclockwise rotation (except for a part of the Aptian centuries (115-125 Ma ago), when the sublatitudinal post-collisional dikes shifted clockwise).

Preprints (www.preprints.org) | NOT PEER-REVIEWED | Posted: 17 August 2023 doi:10.20944/preprints202308.1252.v1

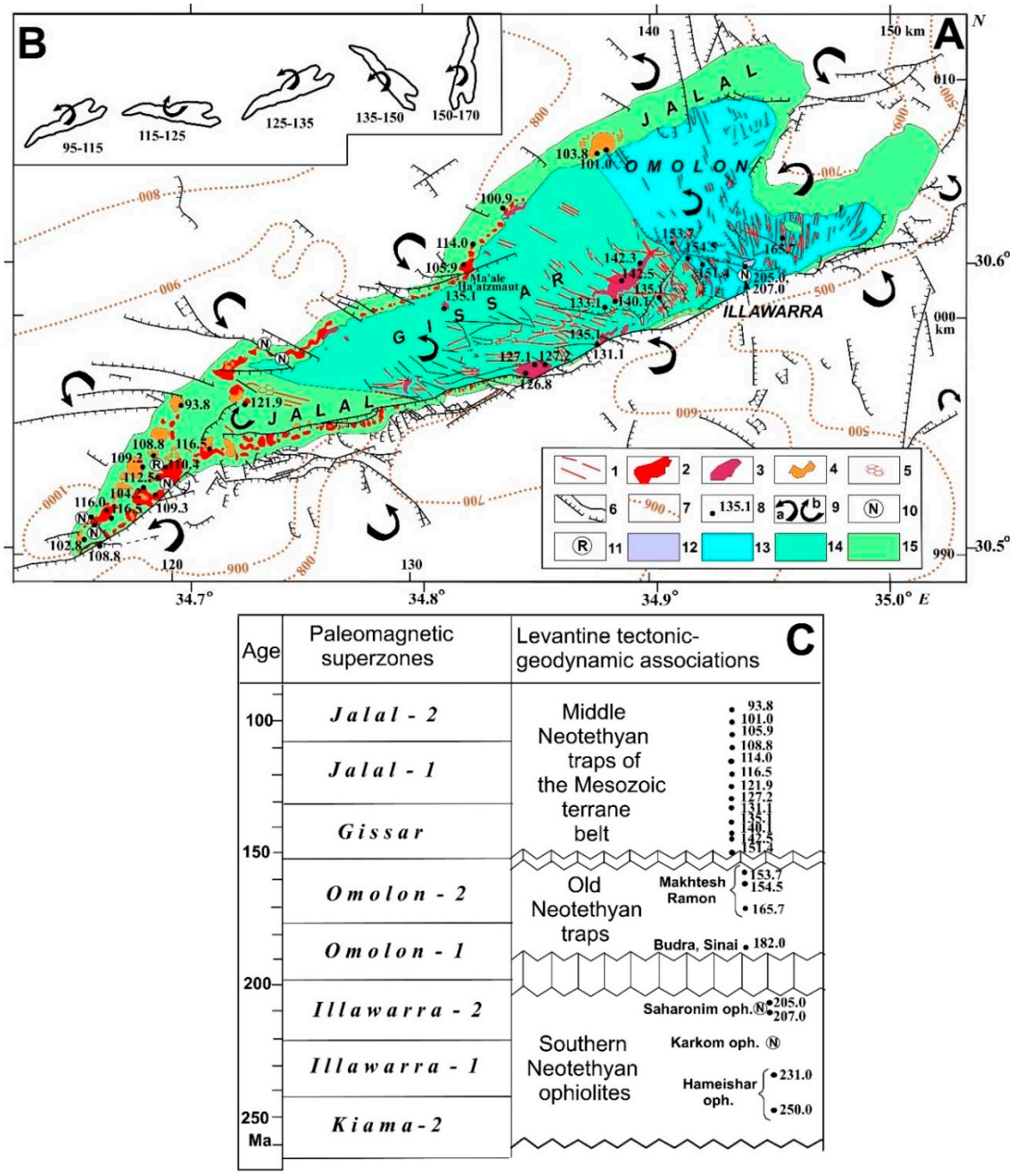

Figure 6. Makhtesh Ramon (Negev Desert, southern Israel) geodynamic-paleomagnetic map (revised and supplemented after Eppelbaum and Katz, 2022). **A**: geodynamic-paleomagnetic indicators. **B**: geodynamic changes of Makhtesh Ramon subterrane displacement in the Middle Mesozoic. **C**: Paleomagnetic scale. (1) precollisional-collisional basalt dikes, (2) postcollisional alcalic olivine basalt flows and volcanoclastic rocks, (3) precollisional association of alcalic olivine gabbro, monzogabbro and syenites, (4) postcollisional association of basanites and nefelinites, (5) quartzitic hexagonal prisms, (6) faults, (7) hypsometric isolines within the Makhtesh Ramon plateau (1-7 from Garfunkel and Katz (1967), Zak (1968), Baer and Reshes (1991), Baer (1993), Sneh et al. (1998), Avni (2001), Zilberman and Avni (2004a, 2004b); Vapnik et al. (2007), Yudalevich et al. (2014), Eppelbaum and Katz (2015), Avni et al. (2016, 2017), Baer et al. (2017), Yudalevich and Vapnik (2018), (8) radiometric age of the magmatic rocks (from Lang and Steinitz (1989), Segev (2000), Segev et al. (2005)), (9) counterclockwise (a) and clockwise (b) rotation of the linear structures (faults, dykes and volcanic ridges), (10)-(11) magmatic rocks with normal (10), and reversal (11) paleomagnetic polarity (from Ron and Baer (1988), Gvirtzman et al. (1996), Baer et al. (1995), (12)-(15) paleomagnetic zonation (classification) of the magmatic complexes: (12) Illawarra, (13) Omolon, (14) Gissar, (15) Jalal.

 doi:10.20944/preprints202308.1252.v1

3.5.3. Hermon area (Northern Israel)

The Hermon Mt., belonging to the Antilebanon terrane, is the most elevated tectonic block of the Easternmost Mediterranean, reaching an absolute elevation of 2,482 m above sea level and with an abnormal increase in the depth of the Moho surface – over 37 km (Eppelbaum et al., 2012). The paleomagnetic map of the Mt. Hermon area is based on an integration of petrological (Shimron and Lang, 1989; Wilson et al., 2000), petrostructural (Shimron and Peltz, 1993), radiometric (Shimron and Lang, 1988, 1989; Lang and Shimron, 1991; Wilson et al., 2000; Segev and Lang, 2002; Frank et al., 2002; Behar et al., 2019) and paleomagnetic (Frank et al., 2002; Behar et al., 2019) and some other data (Figure 7A, B, C). All these data enable us to conclude that within the study area, three paleomagnetic complexes are developed, two of which are Mesozoic (Gissar and Jalal), and one is Late Cenozoic; the youngest zones of the Brunhes and Matuyama relate to the Sogdiana superzone (Figure 7C). The most ancient Gissar superzone is in the central and eastern parts of the region and is composed of Jurassic carbonates. Few radiometric age data for the Gissar dikes in the north give estimations of 140, 132.4, and 130 Ma. To the south, the xenoliths of these rocks were carried by younger volcanoes, and their radiometric ages were 16 determined between 150 and 140 Ma. In the Elazar horizon, the age of conglomerates is determined as 146 Ma (Wilson et al., 2000). These data are in good agreement with the age from the basal part of the Tayasir traps (Wadi Maliah) – 146 and 133.5 Ma (Lang and Mimran, 1985; Segev and Lang, 2002), and with the age of the Um Sabune Middle Miocene basalts conglomerates, 141.9 Ma in the Shelah area, 35 km north of the exit bedrock basites of the Lower Cretaceous (Shaliv, 1991). This tectonic peculiarity is reflected in the inset (Figure 7B), which indicates the counterclockwise rotation of the Antilebanon terrane from the Jurassic to the present time.

Preprints (www.preprints.org) | NOT PEER-REVIEWED | Posted: 17 August 2023 doi:10.20944/preprints202308.1252.v1

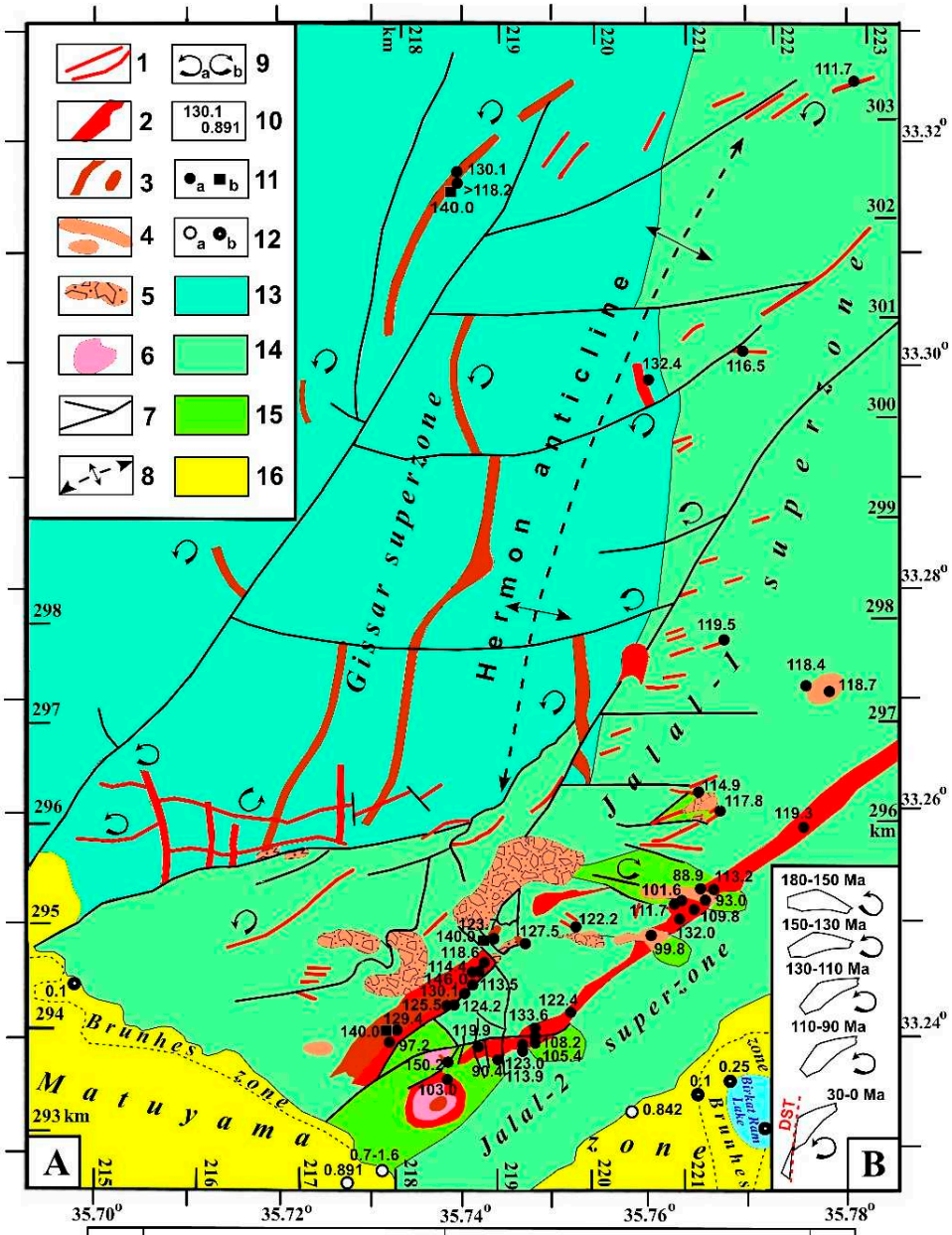

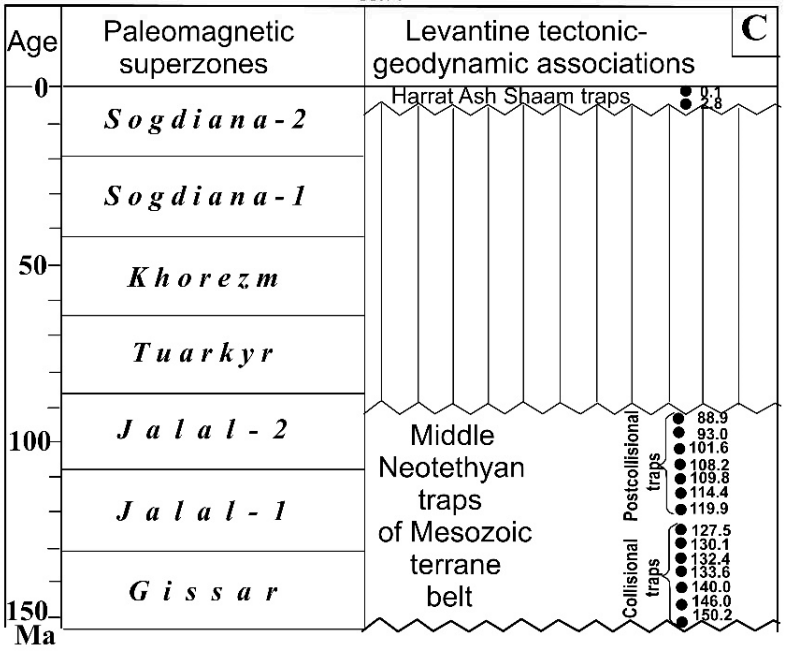

 doi:10.20944/preprints202308.1252.v1

Figure 7. Mt. Hermon geodynamic-paleomagnetic map. **A**: Tectono-paleomagnetic indicators. (1) Lower Cretaceous basalt-basanite dikes, (2) Lower Cretaceous alkaline basalt flows and tuffs, (3) Jurassic - Lower Cretaceous diabase dikes, (4) Lower-Upper Cretaceous alkaline basalt flows, (5) Lower Cretaceous diatreme pipes, (6) Upper Cretaceous alkaline basalt cone, (7) faults, (8) axis of the Hermon anticline, (9) counterclockwise (a) and clockwise (b) rotation of faults and magmatic bodies, (10) radiometric age of magmatic rocks, (11) points of Mesozoic magmatism studied by different methods: (a) by K-Ar, Ar-Ar data, (b) Nd-Sr-Pb isotopic data, (12) paleomagnetic measurements of the Pleistocene magmatic rocks: (a) reverse polarity, (b) normal polarity; ((1–8) and (10–12) from Mor et al., 1997; Shimron and Lang, 1989; Lang and Shimron, 1991; Shimron and Peltz, 1993; Shimron, 1998; Wilson et al., 2000; Segev and Lang, 2002; Segev, 2009; Segev and Sass, 2009; Behar et al., 2019), paleomagnetic zones (13-16): (13) Gissar, (14) Jalal-1, (15) Jalal-2, (16) Sogdiana-2 (Matuyama and Brunhes Chrons). **B**: geodynamic changes of Antilebanon terrane displacement in the Middle Mesozoic – Cenozoic. **C**: Paleomagnetic scale.

3.6. Critical latitude of the Earth

Véronnet's (1912) comprehensive physical-mathematical analysis of the Earth's rotating ellipsoid indicated that the two Earth's critical latitudes are ±≅35°. These effects are due to Earth's rotation velocity changes and the tidal forces' uneven impact (Véronnet, 1912). Further studies using extensive geological-geophysical materials demonstrated that, following Véronnet's theory, periodic matter fluxes in the Earth's mantle move from the equatorial to the polar regions and vice versa (Andersson, 2007; Khain and Koronovsky, 2007). Eppelbaum et al. (2021) showed that the latitude of +35° coincides with the center of the projection of the revealed quasi-circular mantle structure (Figure 2).

3.7. Results of regional seismic tomography studies

The results of deep seismic tomography (Su et al., 1994; Van der Hilst et al., 1997; Wen and Helmberger, 1998; Schmid et al., 2008; van der Meer et al., 2018) indicate abnormal velocities of P- and S-wave propagation at depths of 1200–1800 km beneath the Eastern Mediterranean that also confirm the presence of the giant anomalous target in the lower mantle. The seismic tomographic profile through the Antalya region at 40° N (southern Turkey) clearly indicates heterogeneous sources in the mantle indoors the contour of the recognized huge quasi-ring object at depths of about 1600 km (van der Meer et al., 2018).

3.8. Study of paleobiogeographical data

The counterclockwise rotation of the deep quasi-ring structure and its relationship with the surface (subsurface) sequences can also be confirmed paleobiogeographically. Late Jurassic shallow-water deposits of the Northern, and Southern Palmyrides, Antilebanon, and Negev terranes include coral biostroms with brachiopods and echinoid banks. The brachiopod fauna (*Somalirhynchia-Septirhynchia*) in these facies is very similar to those found in the Ethiopian paleobiogeographical province in Saudi Arabia, Somalia, and Ethiopia (Eppelbaum and Katz, 2015). Thus, the sedimentary deposits of the foreland of Northern Arabia and Eastern Nubia are tectonically discordantly joined with the allochthonous Mesozoic terrane belt rotated counterclockwise towards the Gondwana.

3.9. Mineral-petrological analysis

An overview of the mineral-petrological features of deep origin for the study region designates that many different magmatic indicators are observed in the projection of the mantle structure. The largest number of rocks and minerals of deep origin are concentrated in the apical part of the projection, in the center of which occur the Cyprus ophiolite zones. Here numerous mantle minerals (e.g., melilite, clinopyroxene, amphibole, olivine, Cr-spinels) were found (e.g., George, 1978; Chan et al., 2008; Aldanmaz et al., 2020). The mantle rocks and minerals were identified in: northern Syria (diamonds and kimberlites) (Sharkov and Hanna, 1987), Carmel area (northern Israel) (e.g., ultramafic xenoliths, corundum xenocrysts, mantle peridotites, tistarites, diamonds, moissanite,

 doi:10.20944/preprints202308.1252.v1

eclogites, garnet websterites) (Esperanca and Garfunkel, 1986; Dobrzhinetskaya et al., 2018; Griffin et al., 2016, 2018; Lu et al., 2022); (4) Makhtesh Ramon area (southern Israel) (e.g., moissanite, corundum, diamonds, olivine, perovskites, yttrium phosphate) (Eppelbaum et al., 2006; Vapnik et al., 2007; Yudalevich et al., 2014; Eppelbaum and Vaksman, 2017; Yudalevich and Vapnik, 2018), Central Eastern Desert of Egypt (diamonds, some satellite minerals, and kimberlites) (Barakat and Kandil, 2019).

3.10. Magnetic field analysis

Analysis of the GPS local measurements (Figure 2) and paleomagnetic mapping data (Figure 1) made it possible to establish that the deep mantle structure experiences counterclockwise rotation unambiguously (Eppelbaum et al., 2021). Of course, these data are not based on regional mapping but on disparate data from different parts of a vast sub-oval structure. At the same time, satellite gravimetry data made it possible, on the one hand, to outline the deep mantle oval and reveal the local structures of the Mesozoic terrane belt and other elements of the tectonosphere (Eppelbaum et al., 2021).

In the apical part of the deep structure, it was essential to discover the ancient oceanic crust of the Kiama zone in the Levant (Eppelbaum et al., 2014) and analyze active geodynamics to the north of it, in the Cyprus region (Eppelbaum et al., 2018, 2021). However, these disparate data are significant regarding local shifts and need to provide information about the regional turn of the structure itself. The constructed smoothed map of the vertical component of the magnetic field ΔZ (Figure 8) made it possible for the first time to cartographically show the reality of the apical center rotation in the axial zone of the deep mantle structure of the Eastern Mediterranean. Here is observed a coincidence of regional zones of magnetization with gravity isolines of the oval of deep mantle structure. The magnetic map indicates that the most prominent stress zone is in southeastern Turkey, near the transition of the apical uplift to the wing of the deep structure projection (Figure 8). It can be clearly seen that the residual gravity anomaly, GPS vector behavior, and the magnetic field pattern create a single ensemble. A zone of slightly increased values of the geomagnetic field anomaly with a gentle central trough is developed here. Furthermore, on the periphery of the central uplift, there are scattered troughs discordant concerning the structures of the tectonosphere with negative magnetic anomalies.

Figure 9 displays the magnetic map of the Eastern Mediterranean (this map's coordinates white contoured in Figure 8 and coincide with the gravity gradient map presented in Figure 4). Particularly significant is the fact that in the negative anomaly of Anatolides-Aleppo, there are zones of manifestation of recent catastrophic earthquakes. The discordance of concentric magnetic anomalies concerning the structures of the Mesozoic terrane belt, Arabia, and Anatolia indicates their connection with deep geodynamics. In this regard, the deep tectonic-geodynamic boundary between Eurasia and Gondwana in the North Anatolian Fault (NAF) region is significant for confirming counterclockwise movements of the deep mantle structure. As can be seen from the data on the northwestern end of the map, the most significant positive anomaly, 90 nT, turns to the southwest, which entirely coincides with the regional GPS data (Figure 2).

Preprints (www.preprints.org) | NOT PEER-REVIEWED | Posted: 17 August 2023 doi:10.20944/preprints202308.1252.v1

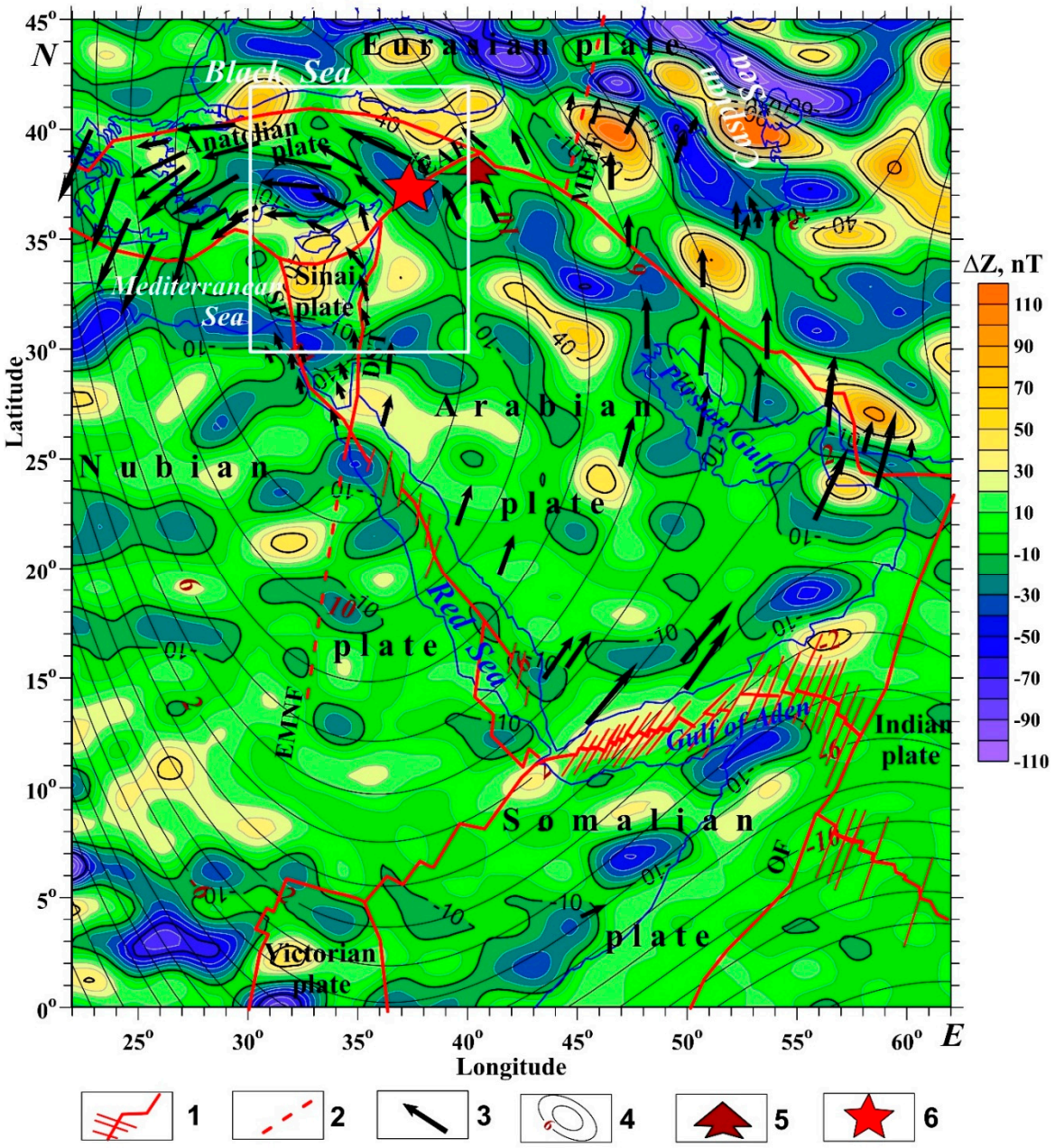

Figure 8. Smoothly averaged magnetic ΔZ map recalculated to one common level of 2.5 km over the msl (initial data from https://geomag.colorado.edu/magnetic-field-model-mf7.html) for African-Arabian region with the main tectonic elements, the behavior of the GPS vectors and overlaid residual gravity anomaly (see Figure 2). The white rectangle contours the magnetic map presented in Figure 9. (1) intraplate faults, (2) interplate faults, (3) GPS vectors, (4) residual gravity field isolines, (5) distal part of the Mesozoic terrane belt, (6) epicenters of two main catastrophic earthquakes in eastern Turkey (February 06, 2023).

Preprints (www.preprints.org) | NOT PEER-REVIEWED | Posted: 17 August 2023 doi:10.20944/preprints202308.1252.v1

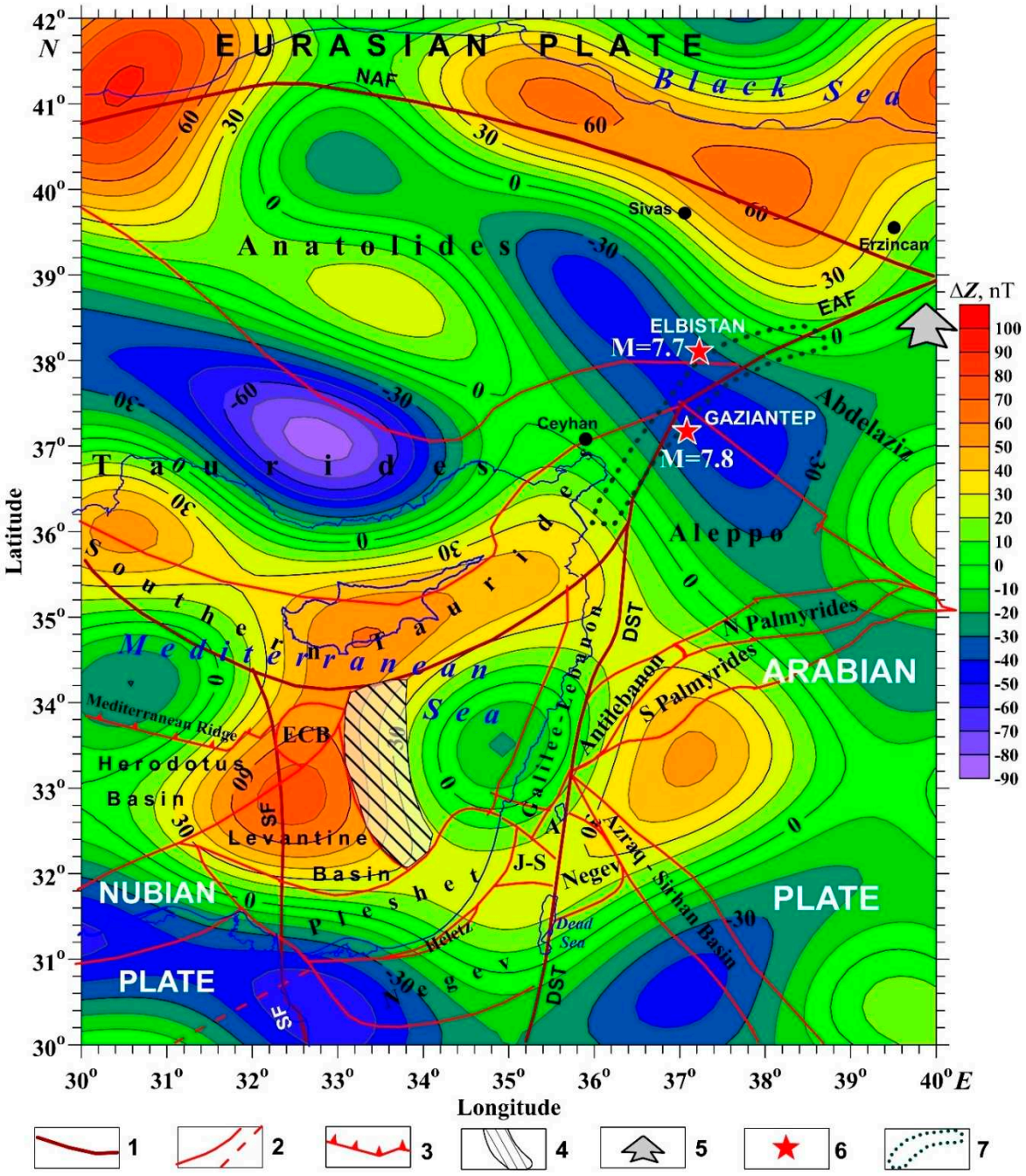

Figure 9. Smoothly averaged magnetic ΔZ map recalculated to one common level of 2.5 km over the msl for the central part of the Easternmost Mediterranean (initial data are from https://geomag.colorado.edu/magnetic-field-model-mf7.html) with the main tectonic elements and seismological features in eastern Turkey. The contour of this map is shown in Figure 8 by a white rectangle. (1) interplate faults, (2) intraplate faults, (3) Mediterranean Ridge, (4) contour of the oceanic crust block relating to the Kiama paleomagnetic hyperzone of inverse polarity, (5) distal part of the Mesozoic terrane belt, (6) epicenters of two main catastrophic earthquakes in eastern Turkey, (7) dangerous seismogenic zone (after Hancilar et al. (2023)). ECB, Eratosthenes Continental Block, DST, Dead Sea Transform, SF, Sinai Fault, J-S, Judea-Samaria, A, Antilebanon, NAF, Northern Anatolian Fault, EAF, Eastern Anatolian Fault.

3.11. Asymmetry of sedimentary basins

Ben-Avraham (1992) and Smit et al. (2010) analyzed the development of asymmetric basins along transforming continental faults on the eastern side of the revealed deep structure projection. Based on our data, we believe that the recognized deep structure influenced the asymmetric structure

 doi:10.20944/preprints202308.1252.v1

of these basins and their left-lateral regional counterclockwise rotation. In the Gulf of Aqaba, three deep-water trough systems have developed from south to north. They have a form of a series of en-echelon troughs and shifted from east to west. This arrangement suggests a combined influence of the shear mechanism and counterclockwise block rotation.

In the Dead Sea region and the Eilat (Israel–Jordan) graben system, the axial part of the graben is confined to the east, while the flattened part of the structure extends to the west (Ben-Avraham, 1992; Garfunkel and Ben-Avraham, 1996). The Dead Sea basin tectonic–geomorphological and magmatic asymmetry on the eastern and western coasts is well known. In contrast, the eastern part of the basin is characterized by higher amplitudes and is more active (Garfunkel and Ben-Avraham, 1996). Based on the general gently arcuate structure of the Dead Sea Transform (DST) (Smit et al., 2010; Sharon et al., 2020), it was proposed a new geodynamic concept to explain the asymmetry of the deep displacement of the graben-like structures (Eppelbaum et al., 2021). Its essence is the regional development of both shear and rotational displacements of tectonic blocks, which is crucial for explaining the asymmetry of the regional basins.

The Sea of Galilee (Lake Kinneret) is located on the DST northern continuation. The axis of the sea's deep-water basin was displaced to its eastern shore, while the axis of its shallow-water basin was moved to the western shore (Eppelbaum et al., 2022). However, analysis of paleomagnetic data (Ron et al., 1984) obtained from areas adjacent to the Galilee region, and results of structural mapping, have detected extensive developments of arcuate faults in the shear zone (Smit et al., 2010). It enabled us to clarify the general dominant nature of the regional movement geodynamics. They are combined with the counterclockwise axial rotation of the Arabian–Nubian continental crustal blocks, which come to an agreement well with the GPS monitoring data. The asymmetry of local sedimentary basins is also accentuated by the geomorphological asymmetry features of the Arabian–Nubian zone of Gondwana in the Late Cenozoic. In its western part (corresponding to the junction of the Red Sea rift zone and Nubian Plate), the hypsometric marks of the plateau and Nile River valley generally do not exceed 500 m. In the eastern part (Arabian–Sinai zone) of the junction of the Nubian Plate with the Red Sea rift zone system and Dead Sea shear zone, the hypsometric marks exceed 500–1,000 m. In the marginal zones of the Arabian and Sinai plates, mountains range with heights of more than 2,000–3,000 m have formed. We suggest that the described phenomenon of regional geomorphological asymmetry on two sides of the Red Sea rift zone is mainly geodynamically determined by the counterclockwise rotation of the region.

3.12. Explanation of the oceanic crust block origin relating to the Kiama paleomagnetic zone

The central part of the Easternmost Mediterranean which is in the central part of the projection of the mantle structure is also associated with anomalously low regional heat flow values (~20–30 mW/m^2) (Artemieva et al., 2006; Elgabry et al., 2012; Eppelbaum and Katz, 2015). We consider this effect as a reflection of the ancient age of the lithosphere in the studied region (Eppelbaum and Katz, 2020). Besides this, low heat flow values also indicate a cooling lithosphere. The uniqueness of this zone is accentuated by the discovery (based on the combined analysis of numerous geological–geophysical data) of one of the most ancient oceanic crust blocks relating to the Kiama paleomagnetic hyperzone of reverse polarity (Late Carboniferous–Early Permian) (Eppelbaum et al., 2014). The upper edges of this block lie at the depths of about 10–11 km at the center of the deep structure projection, a few tens of kilometers south of the Cyprus Island (Eppelbaum et al., 2014; Eppelbaum and Katz, 2015) (Figures 1 and 9). The occurrence of the strongly magnetized Earth's crust block with reverse magnetization between the positive and negative magnetic anomalies in the magnetic map (Figure 9) is explained as a composite combination of inverse magnetization with a complex geometrical form of this block. The initial formation of the Kiama hyperzone block (Eppelbaum and Katz, 2015) could have occurred east of the present position of the Persian Gulf (Hall et al., 2005). Our geodynamic model suggests that this tectonic block was displaced along regional transform faults to its current position under the influence of the deep structure counterclockwise rotation. It can be proposed that the crucial impact of the deep structure just prevented the oceanic block subduction and preserved its location to the present.

 doi:10.20944/preprints202308.1252.v1

4. Brief description of the catastrophic seismic events on 06.02.2023 in Eastern Turkey

4.1. Short seismological-tectonic sketch

The accumulated stress in this area was indicated by many authors (e.g., Tselentis and Drakopoulos, 1990; Ambraseys and Finkel, 1995; Stein et al., 1997; Nalbant et al., 2002; Şengör et al., 2005; Öztürk, 2018; Alpyürür and·Lav, 2022).

The latest catastrophic earthquakes in eastern Turkey require their geodynamic understanding. The two most decisive events (with magnitude (M) = 7.8 and 7.7) (according to the USGS estimations) were observed with an interval of 9 hours on February 06, 2023, followed by a whole series of aftershocks (four with M ≥6, about forty with M ≥5, and more than 200 with M ≥4). The ground acceleration values recorded in some areas near the fault rupture exceeded 1*g* (Baptie and Segou, 2023) and even 2*g* (Çen et al., 2023). A reevaluation of the earthquakes using long-period coda moment magnitude gave values M =7.95±0.013 and M =7.86±0.012, respectively (Jiang et al., 2023), that is, the amplitude of these catastrophic earthquakes was actually even higher. These earthquakes, obviously, were the most enormous Turkish earthquakes in over 2,000 years (KeAi, 2023). According to Karabulut et al. (2023), catastrophic earthquakes were preceded by long seismic silence. This fact indicates a long-term accumulation of seismic stress.

These tragic events led to the death of about 60 thousand people. The above values indicate the colossal tension created in the Earth's crust. The region where these strongest earthquakes occurred is a tectonically very complex junction zone of four tectonic plates: Eurasian, Arabian, African, and Anatolian. The joint movement of these plates (consisting, in turn, of tectonic elements of different ages) occurs at an average rate of 6–15 mm per year. However, after two marked powerful shocks, the Anatolian plate shifted to the southwest by three meters; later, this shifting continued for several (entirely to ~11.5) meters.

4.2. First event of M = 7.8, 06.02.2023

The epicenter of this event at (01:17 UTC) was 37 km west–northwest of Gaziantep (Figure 4) and had a maximal Mercalli intensity of XII. According to the United States Geological Survey (USGS), the earthquake hypocenter was at a depth of 10.0 km. The shock had a focal mechanism relating to strike-slip faulting (National Earthquake …, 2023 I).

A source model for the M = 7.8 seismic event produced by the USGS from observed seismic waves, considering preliminary rupture mapping from satellite data, employed three fault segments. These segments have individual lengths (a), widths (b), strikes (c), and dips (d). Segment 1: (a) >40 km, (b) 30 km, (c) 028°, (d) 85°, Segment 2: (a) >175 km, (b) 30 km, (c) 060°, (d) 85°, Segment 3: (a) >160 km, (b) 20 km, (c) 025°, (d) 75°. The mainshock produced a maximum slip of 11.2 m along segment 2, beneath the Sakarya district in Kahramanmaraş Province, northeast of the junction where it meets segment 1 (National Earthquake …, 2023 I).

4.3. Second event of M = 7.7, 06.02.2023

The first event was followed by M = 7.7 earthquake at 10:24 UTC 95 km north-northeast (Figure 4). It had a depth of 7.4 km, according to the USGS. The shock was also the result of strike-slip faulting (National Earthquake …, 2023 II); it had an epicenter north of the previous large earthquake (Figure 4).

The USGS source model for the M_w 7.7 earthquake that struck nine hours later, has three large fault segments. Segment 1: a >70 km, b > 20 km, (c) 276°, and (d) 80°, Segment 2: a >40 km, b >20 km, (c) 250°, (d) 80°, and Segment 3: (a) ~80 km, b >20 km, (c) 060°, and (d) 80°. The maximum displacement registered on Segment 1 was 11.4 m (National Earthquake …, 2023 II).

4.4. Main tectonic consequences

 doi:10.20944/preprints202308.1252.v1

Thus, the Eastern Turkey land segments were displaced southwest to the Mediterranean Sea (with the maximal movement of 11.2 and 11.4 m), i.e., counterclockwise. This fact agrees with the proposed theory about the influence of the counterclockwise rotating deep quasi-circular structure.

5. Discussion

It was found that the most crucial element of the zone of the junction of the Eurasian and Gondwana platforms is the zone of collision of the Mesozoic terrane belt (MTB) (composed of massifs of thinned continental and oceanic crust) (Eppelbaum and Katz, 2015) and the Alpine-Himalayan orogenic belt (formed of a highly variegated complex of blocks of continental bark and numerous ophiolites). The most complex section of this junction zone corresponds to the distal protrusion of the MTB, which intrudes into the Alpine-Himalayan belt in the eastern area of wedging out of the tectonically most complex part of the Anatolian plate (Figures 4 and 9). Near this junction zone, the sublatitudinal critical Earth's latitude of 35° (Véronnet, 1912) is developed (Eppelbaum et al., 2021).

The tectonic-structural analysis describes the most significant features of the Earth's crust's regional deformation with a sublatitudinal Alpine belt and a submeridional Neoproterozoic belt with an arcuate protrusion of the MTB in the zone of their junction. The combination of tectonic and paleomagnetic data shows (Figure 1) that deep diagonal faults are developed approximately in this zone, near which the rotation of tectonic blocks in the counterclockwise direction dominates in the west, and in the east, in the clockwise direction. The zone of catastrophic earthquakes under consideration is developed west of the arcuate ledge. Geophysical-geodynamic mapping (Figures 1 and 2) using tectonic modeling, GPS data analysis (Reilinger et al., 2006), calculation of a residual satellite gravity anomaly together with the analysis of numerous paleomagnetic (Figures 1 and 5–7), structural-tectonic, petrological, biogeographical, and other data only recently made it possible to obtain a reliable explanation of the geodynamic features and history of the development of the region under consideration (Eppelbaum et al., 2020, 2021). A deep mantle structure rotating in a counterclockwise direction was revealed by a set of geological-geophysical features. In the present paper, this set is extended and supplemented. This phenomenon significantly influenced all geodynamic regional processes in this most complex region, including dangerous geodynamic events. Interestingly, the tectonic map presented in Karabulut et al. (2023) for the Easternmost Mediterranean and Southern Turkey, reflects a quasi-circular pattern.

Figures 1 and 2 show that the most active geodynamic processes are developed in the apical part of the deep structure. In the contact zone of the most active faults (Dead Sea Transform (DST) and Eastern Anatolian Fault (EAF)), deep stresses are discharged in the distal part of the northward-moving Arabian lithospheric plate with the deviation of the focal zones of high-magnitude earthquakes to the south-west, in the direction of movement of the blocks counterclockwise (Figure 1). Therefore, the Anatolian plate was shifted in this direction towards the Mediterranean Sea.

The distribution of GPS vectors (Figure 2), which clearly indicates the counterclockwise rotation, agrees well with the residual gravity anomaly isolines (Figure 2) and testifies to the presence of the so-called geodynamic vortex phenomenon in the Eastern Mediterranean (Eppelbaum and Katz, 2017). The residual satellite gravity anomalies and gravity anomalies observed in Cyprus Island and around it (at the geometric center of the mantle structure projection) and in the Red Sea rift zone (lengthwise the long axis of the mantle structure projection) perfectly match with each other (Figure 3). The Cyprus high-amplitude gravity anomaly (Gass, 1968) occurs at the center of this vortex structure (Figure 3). At the same time, outside of the gravity trend contour, e.g., in the northeast of the region, the GPS vectors by degrees obtain a clockwise direction (Figure 2). This trend is also accompanied by changes in the paleomagnetic vector direction from counterclockwise to clockwise (Figure 1). It is interesting to note that the Santorini volcano, which is located near the critical latitude of 35° N and the center of the mantle structure projection, was the basis of one of the most catastrophic events in world history (17th century BCE) (Eppelbaum and Pilchin, 2005).

Outcrops of various mantle magmatic elements in Cyprus (e.g., George, 1978; Taylor and Nesbitt, 1988; Chan et al., 2008), Carmel area (northern Israel) (e.g., Esperanza and Garfunkel, 1988; Griffin et al., 2016, 2018; Dobrzhinetskaya et al., 2018; Lu et al., 2022), Makhesh Ramon area (southern

Israel) (e.g., Eppelbaum et al., 2006; Vapnik et al., 2007; Yudalevich and Vapnik, 2018), and Central Eastern Desert (Egypt) (e.g., Barakat and Kandil, 2019) testify to high tectonic-geodynamic activity in the near-surface projection of the mantle anomalous zone.

The Red Sea rifting zone is part of a deep fault, which continues northward to the Carpathian region and intersects different lithospheric plates and structures. This fault coincides with the long axis of the deep mantle structure projection. The deep mantle structure's central (apical) part forms the Sinai Plate, bounded meridionally by two faults. In the north, the Sinai Plate is bounded by a fault that stretches from the southern part of the Aegean–Anatolian Plate. The southern part of Cyprus Island, where a Cretaceous mantle diapir reaches the surface, where the oldest oceanic crust block relating to the Kiama hyperzone was discovered (Eppelbaum et al., 2014; Eppelbaum and Katz, 2015). Our data indicate the Red Sea's geodynamic asymmetry between the eastern and western coasts (Eppelbaum et al., 2021), which is caused by the counterclockwise rotation. The summation of these factors enabled a conclusion on the regularity of the phenomena caused by the mantle structure influence.

Eppelbaum et al. (2018) developed a map of the thicknesses of the lithosphere for the studied region. The thickening of the mantle lithosphere is displaced to the east in the direction of counterclockwise rotation of its deep structure to the central region of the Arabian Plate, with a maximum thickness of ≥150 km in the frontal zone of deep movement of masses (Eppelbaum et al., 2018). The thickness minima (~70–75 km) outline the eastern coast of the Red Sea and the zone east of the DST, where the Late Cenozoic traps are developed.

The regional paleomagnetic data (Figure 1), paleomagnetic sketch map (Figure 5), and paleomagnetic-geodynamic maps of Makhtesh Ramon (Figure 6) and Hermon (Figure 7) unambiguously signify the counterclockwise rotation of tectonic blocks in the deep quasi-ring structure projection. This confirms numerous paleomagnetic studies of the Anatolian block and Western Greece (e.g., Le Pichon et al., 1995; Tatar et al., 2004; Faccenna et al., 2006; Gürer et al., 2017). At the same time, the geodynamic instability happening in the peripheral areas of the mantle structure projection causes the appearance of both clockwise and counterclockwise rotations. Outside the mantle structure projection, clockwise rotation prevails.

The first compiled maps of the vertical magnetic component ΔZ (Figures 8 and 9) clearly display a circular behavior of magnetic anomalies in the corresponding regions. Such behavior is an additional solid argument confirming the influence of the rotated mantle structure. These maps indicate the influence of a deep anomalous object on the rocks occurring at depths of no more than several tens of kilometers.

The generalized geoid anomaly map (Eppelbaum et al., 2021) represents a large quasi-ring anomaly that correlates well with the residual gravitational anomaly map and GPS vector distribution (the last two features are shown in Figure 2). The compiled gravity gradient map for the central part of the studied region (including an area of the 06.02.2023 earthquakes) (Figure 4) shows that it can be utilized as an independent tool for monitoring active seismogenic faults.

Trubitsyn's (2010) theoretical calculations confirm the obtained constructions. This author's model indicates that a depth of 1650–1700 km corresponds to the anomalous zone of the spin (phase) transition, which coincides with the calculated upper edge of the discovered mantle structure. Trubitsyn (2012) noted that such zones are the most unstable and often include mantle plumes, which can affect geodynamically and magmatically the upper mantle, crustal blocks, and characteristics of sedimentary basins (last – in near-surface layers).

It is fascinating to note that many authors (Skobelin et al., 1990; Khain, 2001) argue that conventional plate tectonics cannot explain the intraplate (platform) magmatism (traps, flood basalts, kimberlites) and the related metallogeny. Nevertheless, the identified rotating mantle structure can theoretically explain the origin of linear structures of continental magmatism, which remains insufficiently substantiated in the tectonic-geophysical aspect (Skobelin et al., 1990).

The constructed combined physical–geological model verifies the existence of the giant mantle rotating quasi-ring structure and is based on the following geophysical–geological factors integration: (1) calculation of the residual gravity anomaly displaying the contour of the circular

(ellipsoidal) structure, (2) the results of quantitative analysis of the residual gravity anomaly indicating its depth, (3) quasi-circular behavior of the GPS vector distribution, (4) geoid's anomalous pattern coinciding with the items (1) and (3), (5) seismotomographic data displaying the anomalous medium characteristics in the lower mantle of the region under study, (6) paleomagnetic data doubtless indicating predominant counterclockwise rotation of crustal blocks, (7) circular ΔZ magnetic field pattern at the level of 2.5 km over the msl, repeating mainly the residual gravity and GPS designs, (8) numerous petrological and mineralogical data designating the tectonic and geodynamic activity within the deep mantle projection onto the near-surface part of the geological section, (9) geodynamic conclusions about the conjugate deformation of the Earth's ellipsoid along the critical latitude of +35°, where the center of the revealed deep target is located, (10) paleobiogeographic data analysis indicating the counterclockwise rotation of the surface (near-surface) layers, (11) numerous tectonic-geodynamic data (first of all, results of the last catastrophic earthquakes in Eastern Turkey, when the large land segments were displaced counterclockwise).

Using the trivial notions from the theory of probability, it is improbable that these independent significant factors accidentally coincide (given that we consider only the main indicators) (e.g., Ash, 2008).

6. Conclusions

This multi-method study sheds light on the relationship between the revealed mantle structure and different subsurface geological-geophysical features. The probabilistic estimate of a random coincidence of all these factors, listed in the Discussions, is extremely small. We believe that this structure influenced to the origin of the Cyprus high-amplitude gravity anomaly, the Sinai Plate configuration, the counterclockwise rotation of the Mesozoic terrane belt, the geometry of asymmetric basins along the Dead Sea Transform, and the displacement of the tectonic block corresponding to the Kiama paleomagnetic hyperzone in the Eastern Mediterranean. The discovery of a deep anomalous structure explains the existence of intraplatform magmatic belts that had not previously found explanations within the framework of existing theories. This mantle rotating ring structure, influencing many tectonic–geodynamic processes, maybe a global geodynamic factor contributing to the spreading of the Red Sea. Finally, we propose that just the giant accumulated stress caused by the deep mantle structure's counterclockwise rotation was the main reason for the catastrophic Turkish earthquakes on February 06, 2023.

References

1. Aldanmaz, E., van Hinsbergen, D.J.J., Yıldız-Yüksekol, Ö., Schmidt, M.W., McPhee, P.J., Meisel, T., Güçtekin, A. and Mason, P.R.D., 2020. Effects of reactive dissolution of orthopyroxene in producing incompatible element depleted melts and refractory mantle residues during early fore-arc spreading: constraints from ophiolites in Eastern Mediterranean. *Lithos*, **360–361**, 105438, 1-14. https://doi.org/10.1016/j.lithos.2020.105438
2. Aleinikov, A.L., Belikov, V.T. and Eppelbaum, L.V., 2001. Some Physical Foundations of Geodynamics (in Russian, contents, and summary in English). *Kedem Printing-House*, Tel Aviv, Israel.
3. Alpyürür, M. and·Lav, M.A., 2022. An assessment of probabilistic seismic hazard for the cities in Southwest Turkey using historical and instrumental earthquake catalogs. *Natural Hazards*, **114**, 335-365. https://doi.org/10.1007/s11069-022-05392-x
4. Ambraseys, N.N. and Finkel, C.F., 1995. *Seismicity of Turkey and adjacent areas: a historical review, 1500–1800*. Eren Yayinlari Publ., 240 p.
5. Andersson, D.L., 2007. *New Theory of the Earth*, 2nd ed. Cambridge Univ. Press, Cambridge.
6. Artemieva, I., Thybo, H. and Kaban, M.K., 2006. Deep Europe today: Geophysical synthesis of the upper mantle structure and lithospheric processes over 3.5 Ga. In: (D.G. Gee and R.A. Stephenson, Eds.), *European Lithosphere Dynamics*, Vol. 32 of *Geol. Soc. London., Mem.*, 11–41. https://doi.org/10.1144/GSL.MEM.2006.032.01.02
7. Ash, R.B., 2008. *Basic Probability Theory*. Dover Publications, Inc. Mineola, N. Y., 350 p.
8. Avni, Y., 2001. Har Loz, Sheet 21-III. Geological Map of Israel 1:50,000, *Geol. Survey of Israel*, Jerusalem.
9. Avni, Y., Bartov, Y. and Shen, A., 2016. Har Ardon, Sheet 22-I. Geological Map of Israel 1:50,000, *Geol. Survey of Israel*, Jerusalem.

10. Avni, Y., Beker, A. and Zilberman, E., 2017. Be'erot Oded, Sheet 21-IV. Geological Map of Israel 1:50,000, *Geol. Survey of Israel*, Jerusalem.
11. Baer, G., 1993. Flow directions in sills and dikes and formation of cauldrons in eastern Makhtesh Ramon. *Israel Jour. of Earth Sci*., **42**, 133-148.
12. Baer, G., Heimann, A., Eshet, Y., Weinberger, R., Mussett, A. and Sherwood, G., 1995. The Saharonim Basalt: A Late Triassic – Early Jurassic intrusion in southeastern Makhtesh Ramon, Israel. *Israel Jour. of Earth Sci*., **44**, 1-10.
13. Baer, G. and Reches, Z., 1991. Mechanics of emplacement and tectonic implications of the Ramon dike systems, Israel. *Jour. of Geophysical Research*, **96**(B7), 11895-11910. https://doi.org/10.1029/91JB00371
14. Baer, Y., Soudry, D., Bar, O. and Shen, A., 2017. Zofar, Sheet 22-III, IV. Geological Map of Israel 1:50,000, *Geol. Survey of Israel*, Jerusalem.
15. Baptie, B. and Segou, M., 2023. The Kahmaran Maras earthquake sequence, Turkey/Syria. British Geological Survey (14 Febr. 2023). Retrieved 18 July 2023.
16. Barakat, A.A.S. and Kandil, M.R., 2019. Diamond in the newly discovered kimberlite and related rocks, Central Eastern Desert, Egypt. *Proceed. of the XXXVI Intern. Conf. "Magmatism of the Earth and Related Strategic Metal Deposits"*, St. Petersburg, Russia, 36–42.
17. Barbeau, E.J., 2003. *Polynomials*. Springer, New York.
18. Barka, A. and Reilinger, R., 1997. Active tectonics of the Eastern Mediterranean region: deduced from GPS, neotectonic, and seismicity data. *Ann. Geophys*., **40**, 587-610.
19. Bazhenov, M.L. and Burtman, V.S., 2002. Eocene paleomagnetism of the Caucasus (southwest Georgia): Oroclinal bending in the Arabian syntaxis. *Tectonophysics*, **344**, 247-259. https://doi.org/10.1016/S0040-1951(01)00189-5
20. Behar, G., Shaar, R., Tauxe, L., Asefaw, H., Ebert, Y., Heimann, A., Koppers, A.A.P. and Ron, H., 2019. Paleomagnetism and paleosecular variations from the Plio-Pleistocene Golan Heights volcanic plateau, Israel. *Geochemistry, Geophysics, Geosystems*, 4319-4334, https://doi.org/10.1029/2019GC008479
21. Ben-Avraham, Z., 1992. Development of asymmetric basins along continental transform faults. *Tectonophysics*, **215**, 209-220. https://doi.org/10.1016/0040-1951(92)90082-H
22. Ben-Avraham, Z., Schattner, U., Lazar, M., Hall, J.K., Ben-Gai, Y., Neev, D. and Reshef, M., 2006. Segmentation of the Levant continental margin, eastern Mediterranean. *Tectonics*, **25**, TC5002, 1-17. https://doi.org/10.1029/2005TC00182426
23. Borradaile, G.J., Lagroix, F., Hamilton, T.D. and Trebilcock, D.A., 2010. Ophiolite tectonics, rock magnetism and paleomagnetism, Cyprus. *Surv. Geophys*., **31**, 285-359. https://doi.org/10.1007/s10712-009-9090-2
24. Boschi, L., Faccenna, C. and Becker, T.W., 2010. Mantle structure and dynamic topography in the Mediterranean basin. *Geophys. Res. Lett*., **37**, L20303, 1-5. https://doi.org/10.1029/2010GL045001
25. Bosworth, W., Huchon, P. and McClay, K., 2005. The Red Sea and Gulf of Aden Basins. *Jour. of Afr. Earth Sci*., **43**, 334-378. https://doi.org/10.1016/j.jafrearsci.2005.07.020
26. Çabuk, B.S. and Cengiz, M., 2021. Paleomagnetic rotations in the circum-Marmara region, northwestern Turkey since the Late Cretaceous. *Jour. of Asian Earth Sci*., **213**, 104748, 1-15. https://doi.org/10.1016/j.jseaes.2021.104748
27. Çen, K.Ö., Bray, J.D., Frost, J.D., Hortacsu, A., Miranda, E., Moss, R.E.S. and Stewart, J.P., 2023. February 6, 2023 Türkiye Earthquakes: Report on Geoscience and Engineering Impacts. (GEER Association Report 082 ed., 6 May 2023). Earthquake Engin. Research Inst. https://doi.org/doi:10.18118/G6PM34
28. Chan, G.H.-N., Malpas, J., Xenophontos, C. and Lo, C.-H., 2008. Magmatism associated with Gondwanian rifting and Neo-Tethyan oceanic basin development: Evidence from the Mamonia Complex, SW Cyprus. *Jour. of Geol. Soc.* (London, U.K.), **165**, 699-709. https://doi.org/10.1144/0016-76492007-050
29. Cloetingh, S. and Willet, S.D., 2013. Linking deep Earth and surface processes. *EOS*, Trans. Am. Geophys. Union, **94**, 53-54. https://doi.org/10.1002/2013EO050002
30. Cloetingh, S., Tibaldi, A., Dobrzhinetskaya, L., Matenco, L., Nader, F. and de Vries, B. v. W., 2018. From the deep Earth to the surface: A multiscale approach. *Global Planet. Change*, **171**, 1-322.
31. Dobrzhinetskaya, L., Mukhin, P., Wang, Q., Wirth, R., O'Bannon, E., Zhao, W., Eppelbaum, L. and Sokhonchuk, T., 2018. Moissanite (SiC) with metal-silicide and silicon inclusions from tuff of Israel: Raman spectroscopy and electron microscope studies. *Lithos*, **310-311**, 355-368. https://doi.org/10.1016/j.lithos.2017.04.001
32. Doubre, C., Deprez, A., Masson, F., Socquet, A., Lewi, E., Grandin, R., Nercessian, A., Ulrich, P., De Chabalier, J.-B., Saad, I., Abayazid, A., Peltzer, G., Delorme, A., Calasis, E. and Wright, T., 2017. Current deformation in Central Afar and triple junction kinematics deduced from GPS and InSAR measurements. *Geophys. Jour. Intern*., **208,** 936-953. https://doi.org/10.1093/gji/ggw434
33. Duermeijer, C.E., Krijgsman, C.E., Langereis, C.G. and Ten Veen, J.H., 1998. Post-early Messinian counterclockwise rotations on Crete: Implications for Late Miocene to recent kinematics of the southern Hellenic arc. *Tectonophysics*, **298**, 177-189. https://doi.org/10.1016/S0040-1951(98)00183-8

34. Elgabry, M., Panza, G.F., Badawy, A.A. and Korrat, I.M., 2012. Imaging a relic of complex tectonics: the lithosphere-asthenosphere structure in the Eastern Mediterranean. *Terra Nova*, **25**, No. 2, 102-109. https://doi.org/10.1111/ter.12011
35. Eppelbaum, L.V., Katz, Y.I. and Ben-Avraham, Z., 2012. Israel – Petroleum Geology and Prospective Provinces. *AAPG European Newsletter*, No. 4, 4-9.
36. Eppelbaum, L.V., Ben-Avraham, Z., Katz, Y., Cloetingh, S. and Kaban, M., 2020. Combined Multifactor Evidence of a Giant Lower-Mantle Ring Structure Below the Eastern Mediterranean. *Positioning*, **11**, 11–32. https://doi.org/10.4236/pos.2020.112002
37. Eppelbaum, L.V., Ben-Avraham, Z., Katz, Y., Cloetingh, S. and Kaban, M., 2021. Giant quasi-ring mantle structure in the African-Arabian junction: Results derived from the geological-geophysical data integration. *Geotectonics* (Springer), **55**, No. 1, 67–93. https://doi.org/10.1134/S0016852121010052
38. Eppelbaum, L.V., Nikolaev, A.V. and Katz, Y.I., 2014. Space location of the Kiama paleomagnetic hyperzone of inverse polarity in the crust of the eastern Mediterranean. *Doklady Earth Sciences* (Springer), **457**, No. 6, 710-714. https://doi.org/10.1134/S1028334X14080212
39. Eppelbaum, L.V. and Katz, Y.I., 2012. Key features of seismo-neotectonic pattern of the Eastern Mediterranean. *Izvestiya, Acad. Sci. Azerb. Rep*., Ser.: Earth Sci., No. 3, 29-40.
40. Eppelbaum, L.V. and Katz, Yu.I., 2015. Eastern Mediterranean: Combined geological-geophysical zonation and paleogeodynamics of the Mesozoic and Cenozoic structural-sedimentation stages. *Marine and Petroleum Geol*., **65**, 198–216. https://doi.org/10.1016/j.marpetgeo.2015.04.008
41. Eppelbaum, L.V. and Katz, Yu.I., 2017. A New Regard on the Tectonic Map of the Arabian-African Region Inferred from the Satellite Gravity Analysis. *Acta Geophysica*, **65**, 607-626. https://doi.org/10.1007/s11600-017-0057-2
42. Eppelbaum, L. and Katz, Yu., 2020. Significant tectono-geophysical features of the African-Arabian tectonic region: An overview. *Geotectonics* (Springer), **54,** No. 2, 266-283. https://doi.org/10.1134/S0016852120020041
43. Eppelbaum, L.V. and Katz, Y.I., 2022. Paleomagnetic-geodynamic mapping of the transition zone from ocean to the continent: A review. *Applied Sciences*, **12**, Spec. Issue: ***Advances in Applied Geophysics***, 1-20. https://doi.org/10.3390/app12115419
44. Eppelbaum, L.V., Katz, Y.I. and Ben-Avraham, Z., 2022. Advanced combined geophysical-geological mapping of the Sea of Galilee and its vicinity, In: (A. di Mauro, A. Scozzari, S. Soldovieri, Eds.), *Instrumentation and Measurement Technologies for Water Cycle Management*, Springer, 553-579. https://doi.org/10.1007/978-3-031-08262-7_23
45. Eppelbaum, L., Katz, Yu., Klokochnik, J., Kosteletsky, J., Zheludev, V. and Ben-Avraham, Z., 2018. Tectonic Insights into the Arabian-African Region Inferred from a Comprehensive Examination of Satellite Gravity Big Data. *Global and Planetary Change*, **171**, 65–87. https://doi.org/10.1016/j.gloplacha.2017.10.011
46. Eppelbaum, L.V. and Khesin, B.E., 2012. *Geophysical Studies in the Caucasus*. Springer, Heidelberg.
47. Eppelbaum, L.V. and Pilchin, A.N., 2005. Quick subsidence of a crustal block in SW Aegean Sea as a possible cause of the end of ancient civilization in the 17th century BC. *Trans. of the Intern. Conf. "Atlantis Hypothesis: Searching for a Lost Land"*, Milos Island, Greece.
48. Eppelbaum, L.V. and Vaksman, V.L., 2017. Makhtesh Ramon Complex Deposit (Southern Israel)– A Window to the Upper Mantle. *Intern. Journal of Mining Sciences*, **3**, No. 1, 1-28. http://dx.doi.org/10.20431/2454-9460.0301001
49. Eppelbaum, L.V., Vaksman, V.L., Kouznetsov, S.V., Sazonova, L.M., Smirnov, S.A., Surkov, A.V., Bezlepkin, B., Katz, Y., Korotaeva, N.N., and Belovitskaya, G., 2006. Discovering of microdiamonds and minerals-satellites in Canyon Makhtesh Ramon (Negev desert, Israel). *Doklady Earth Sciences* (*Springer*), **407**, No. 2, 202-204. https://doi.org/10.1134/S1028334X06020097
50. Esperanca, S. and Garfunkel, Z., 1986. Ultramafic xenoliths from the Mt. Carmel area (Karem Maharal volcano), Israel. *Lithos*, **19**, No. 1, 43–49. https://doi.org/10.1016/0024-4937(86)90014-9
51. Faccenna, C., Becker, T.W., Auer, L., Billi, A., Boschi, L., Brun, J.P., Capitanio, F.A., Funiciello, F., Horvàth, F., Jolivet, L., Piromallo, C., Royden, L., Rossetti, F. and Serpelloni, E., 2014. Mantle dynamics in the Mediterranean. *Review of Geophysics*, **52**, 283–332. https://doi.org/10.1002/2013RG000444
52. Faccenna, C., Bellier, O., Martinod, J., Piromallo, C. and Regard, V., 2006. Slab detachment beneath eastern Anatolia: A 10 possible cause for the formation of the North Anatolian fault. *Earth Planet. Sci. Lett*., **242**, 85-97. https://doi.org/10.1029/2002JB001757.
53. Faccenna, C., Jolivet, L., Piromallo, C. and A. Morelli, 2003. Subduction and depth of convection in the Mediterranean mantle. *Jour. of Geophys. Res*.: Solid Earth, **108**, 1-13. https://doi.org/10.1029/2001JB001690
54. Frank, U., Schwab, M.J. and Negendank, J.F.W., 2002. A lacustrine record of paleomagnetic secular variations from Birkat Ram, Golan Heights (Israel) for the last 4400 years. *Phys. Earth Planet. Inter*., **133**, 21-34. https://doi.org/10.1016/S0031-9201(02)00085-7
55. Garfunkel, Z. and Ben-Avraham, Z., 1996. The structure of the Dead Sea basin. *Tectonophysics*, **266**, 155-176. https://*doi*.org/10.1016/S0040-1951(96)00188-6

56. Garfunkel, Z. and Katz, A., 1967. New magmatic features in Makhtesh Ramon, southern Israel. *Geological Magazine*, **104** (No. 6), 608-629. https://doi.org/10.1017/S0016756800050275
57. Garini, E. and Gazeras, G., 2023. The 2 earthquakes of February 6th, 2023, in Turkey. Preliminary Report. NTUA, Greece.
58. Gass, I.G. and Masson-Smith, D., 1963. The geology and gravity anomalies of the Troodos Massif, Cyprus. *Philos. Trans. R. Soc*. London, Ser. A **255**, 417-466. https://doi.org/10.1098/rsta.1963.0009
59. George, R.P., Jr., 1978. Structural petrology of the Olympus ultramafic complex in the Troodos ophiolite, Cyprus. *Geol. Soc. Amer. Bull*., **89**, 845-865). https://doi.org/10.1130/0016-7606(1978)89<845:SPOTOU>2.0.CO;2
60. Griffin, W.L., Gain, S.E.M., Adams, D.T., Huang, J.-X., Saunders, M., Toledo, V., Pearson, N.J. and O'Reilly, S.Y., 2016. First terrestrial occurrence of tistarite (Ti_2O_3): Ultra-low oxygen fugacity in the upper mantle beneath Mount Carmel, Israel. *Geology*, **44**, 815-818. https://*doi*.org/10.1130/G37910.1
61. Griffin, W.L., Gain, S.E.M., Huang, J.-X., Belousova, E.A., Toledo, V. and O'Reilly, S.Y., 2018. Permian to quaternary magmatism beneath the Mt Carmel area, Israel: Zircons from volcanic rocks and associated alluvial deposits. *Lithos*, **314-315**, 307-322. https://doi.org/10.1016/j.lithos.2018.06.007
62. Gvirtzman, G., Weissbrod, T., Baer, G. and Brenner, J., 1996. The age of Aptian stage and its magmatic events: New Ar-Ar ages and paleomagnetic data from the Negev, Israel. *Cretaceous Research*, **17**, 293-310. https://doi.org/10.1006/CRES.1996.0021
63. Gürer, D., van Hinsbergen, D.J.J., Özkaptan, M., Creton, I., Koymans, M.R., Cascella, A. and Langereis, C.G., 2017. Paleomagnetic constraints on the timing and distribution of Cenozoic rotations in Central and Eastern Anatolia. *Solid Earth Discuss*., https://doi.org/10.5194/se-2017-66
64. Hancilar et al. (2023). Kahramanmaraş - Gaziantep Türkiye M7.7 Earthquake, 6 February 2023. Strong Ground Motion and Building Damage Estimations. *Preliminary Report*. Dept. of Earthquake Engineering, Bogazici University, Turkey.
65. Hall, J.K., Krasheninnikov, V.A., Hirsch, F., Benjamini, C. and Flexer, A., 2005. *Geological Framework of the Levant*, Vol. 2: *The Levantine Basin and Israel*. Historical Productions-Hall, Jerusalem, Israel.
66. Henry, B., Homberg, C., Mroueh, M., Hamdan, W. and Higazi, W., 2010. Rotations in Lebanon inferred from new palaeomagnetic data and implications for the evolution of the Dead Sea Transform system. In (C. Homberg and M. Bachman, Eds.), *Evolution of the Levant Margin and Western Arabia Platform since the Mesozoic*, Vol. 341 of Geol. Soc. London, Spec. Publ., 269-285. https://doi.org/10.1144/SP341.13
67. Hisarli, Z.Z.M., 2011. New paleomagnetic constraints on the Late Cretaceous and Early Cenozoic tectonic history of the Eastern Pontides. *Jour. of Geodynamics*, **52**, 114–128. https://doi.org/10.1016/j.jog.2010.12.004
68. Jolivet, L., Faccenna, L., Agard, P., de Lamotte, D. F., Menant, A., Sternai, P. and Guillocheau, F., 2016. Neo-Tethys geodynamics and mantle convection: From extension to compression in Africa and a conceptual model for obduction. *Can. J. Earth Sci*., **53**, 1-15. https://doi.org/10.1139/cjes-2015-0118
69. *Jiang, X., Song, X., Li, T. and Wu, K., 2023.* Special focus/Rapid Communication Moment magnitudes of two large Turkish earthquakes on February 6, 2023, from long-period coda. *Earthquake Science, **36** (2),169–174.* https://doi.org/10.1016/j.eqs.2023.02.008.
70. Kaban, M.K., El Khrepy, S., Al-Arifi, N., Tesauro, M. and Stolk, W., 2016. Three-dimensional density model of the upper mantle in the Middle East: Interaction of diverse tectonic processes. *Jour. of Geophys. Res*., Ser.: Solid Earth, **121**, 5349-5364. https://doi.org/10.1002/2015JB012755
71. Karabulut, H., Güvercin, S.E., Hollingsworth, J. and Konca1, A.Ö., 2023. Long silence on the East Anatolian Fault Zone (Southern Turkey) ends with devastating double earthquakes (6 February 2023) over a seismic gap: implications for the seismic potential in the Eastern Mediterranean region. *Jour. of the Geological Society*, London, **180**, 1-10. https://doi.org/10.1144/jgs2023-021
72. *KeAi, 2023.* The magnitude of the 2023 Turkish earthquake matches the largest in the country's history, according to new study *(11 April 2023). Phys.org.* Retrieved 18 July 2023.
73. Khain, V.E., 2001. *Tectonics of Continents and Oceans*. Nauchnyi Mir, Moscow (in Russian).
74. Khain, V.E. and Koronovskii, N.V., 2007. *Planet Earth: From the Core to The Ionosphere*. Moscow. State. Univ., Moscow (in Russian).
75. Khalafly, A.A., 2006. *Paleomagnetism of the Lesser Caucasus*. Takhsil, Baku (n Russian).
76. Khesin, B.E., Alexeyev, V.V. and Eppelbaum, L.V., 1996. *Interpretation of Geophysical Fields in Complicated Environments*. Modern Approaches in Geophysics, Vol. 14, Kluwer, Dordrecht, 368 p.
77. Khramov, A.N., 1984. *Paleomagnetic Directions and Pole Positions: Data for the USSR (Catalogue)*, No. 1 of *World Data Center, Ser. B*, Geophys. Comm. Acad. Sci. SSSR, Moscow.
78. Kissel, C. and Laj, C., 1988. *Paleomagnetic Rotations and Continental Deformation*. NATO ASI Series: Mathematical and Physical Sciences. Kluwer Academic Publishers: Dordrecht, The Netherlands; Boston, USA; London, UK, 530 p.
79. Kissel, C., Laj, C., Poisson, A. and Gorur, N., 2003. Paleomagnetic reconstruction of the Cenozoic evolution of the Eastern Mediterranean. *Tectonophysics*, **362**, 199-217. https://doi.org/10.1016/S0040-1951(02)00638-8

80. Lang, B. and Mimran, Y., 1985. An Early Cretaceous volcanic sequence in central Israel and its significance to the absolute date of the base of the Cretaceous. *J. of Geology*, **93**, 179-184. https://doi.org/10.1086/628939.
81. Lang, B. and Shimron, A.E., 1991. New K-Ar data of the Mount Hermon Mesozoic magmatic rocks. *Ministry of Energy and Infrastructure*, Geol. Surv. Israel, *Min. Energy Resources Division*, Report GSI/26/91.
82. Lang, B. and Steinitz, G., 1989. K-Ar dating of Mesozoic magmatic rocks in Israel: A review. *Isr. Jour. of Earth Sci*., **38**, 89-103.
83. Lazos, I., Sboras, S., Chousianitis, K., Kondopoulou, D., Pikridas, C., Bitharis, S. and Pavlides, S., 2022. Temporal evolution of crustal rotation in the Aegean region based on primary geodetically-derived results and palaeomagnetism. *Acta Geodaetica et Geophysica*, **57**,317–334. https://doi.org/10.1007/s40328-022-00379-3
84. Le Pichon, X., Chamot-Rooke, N., Lallemant, S., Noomen, R. and Veis, G., 1995. Geodetic determination of the kinematics of central Greece with respect to Europe: Implications for eastern Mediterranean tectonics. *Jour. of Geophysical Research*, **100**, B7, 12,675-12,990. https://doi.org/10.1029/95JB00317
85. Lotfi, H.I., 2015. Early Cretaceous counterclockwise rotation of Northeast Africa within the equatorial zone: Paleomagnetic study on Mansouri ring complex, Southeastern Desert, Egypt. *NRIAG J. Astron. Geophys*., **4**(1), 1-15.
86. Lu, J.-G., Griffin, W.L., Huang, J.-X., Dai, H.-K., Castillo-Oliver, M., O'Reily, S.Y., 2022. Structure and composition of the lithosphere beneath Mount Carmel, North Israel. *Contrib. to Mineralogy and Petrology*, **177**, 29, 1-16. https://doi.org/10.1007/s00410-022-01897-7
87. McElhinny, M.W., 1989. *Paleomagnetism and Plate Tectonics*. Cambridge Univ. Press, 235 p.
88. Makris, J., Henke, C.H., Egloff, F. and Akamaluk, T., 1991. The gravity field of the Red Sea and East Africa. *Tectonophysics*, **198**, 369-381. https://doi.org/10.1016/0040-1951(91)90161-K
89. Mao, W. and Zhong, S., 2021. Constraints on mantle viscosity from intermediate-wavelength geoid anomalies in mantle convection models with plate motion history. *Jour. of Geoph. Research*: Solid Earth, **126**, e2020JB021561, 1-25. https://doi. org/10.1029/2020JB021561
90. Marchev, P., Raicheva, R., Downes, H., Vaselli, O., Chiaradia, M. and Moritz, R., 2004. Compositional diversity of Eocene–Oligocene basaltic magmatism in the Eastern Rhodopes, SE Bulgaria: Implications for genesis and tectonic setting. *Tectonophysics*, **393**, 301-328. https://doi.org/10.1016/j.tecto.2004.07.045
91. McClusky, S. et al., 2000. Global Positioning System constraints on plate kinematics and dynamics in the eastern Mediterranean and Caucasus. *Jour. of Geophys. Res*., **105**, 5695-5719. https://doi.org/10.1029/1999JB900351
92. Molostovsky, E.A., Pechersky, D.M. and Frolov, I.Yu., 2007. Magnetostratigraphic Timescale of the Phanerozoic and Its Description Using a Cumulative Distribution Function. *Izvestiya, Physics of the Solid Earth*, **43**(10), 811–818. https://doi.org/10.1134/S1069351307100035
93. Mor, D., Mihelson, H., Druckman, Y., Mimran, Y., Heimann, A., Goldberg, M. and Sneh, A., 1997. Notes on the geology of Golan Heights. *Report GSI/15/97*, Jerusalem, 1-18.
94. Morris, A., Erson, M.W., Robertson, A.H. and Al-Riyami, K., 2002. Extreme tectonic rotations within an eastern Mediterranean ophiolite (Baer–Bassit, Syria). *Earth Planet. Sci. Lett*., **202**, 247-261. https://doi.org/10.1016/S0012-821X(02)00782-3
95. Muttoni, G., Kent, D.V., Garzanti, E., Brack, P., Abrahamsen, N. and Gaetani, M., 2003. Early Permian Pangea 'B' to Late Permian Pangea 'A'. *Earth Planet. Sci. Lett*., **215**, 379-394. https://doi.org/10.1016/S0012-821X(03)00452-7
96. Nalbant, S.; McCloskey, J., Steacy, S. and Barka, A.A., 2002. Stress accumulation and increased seismic risk in eastern Turkey. *Earth and Planet Sci. Lett*., **195**, 291-298. https://doi.org/10.1016/S0012-821X(01)00592-1
97. National Earthquake Information Center (6 February 2023). M 7.8 - Kahramanmaras Earthquake Sequence I. United States Geological Survey. Archived from the original on 6 February 2023. Retrieved 15 July 2023.
98. National Earthquake Information Center. M 7.5 – Kahramanmaras Earthquake Sequence II. United States Geological Survey. Archived from the original on 6 February 2023. Retrieved 15 July 2023.
99. Nur, A., Ron, H. and Scott, O., 1989. Mechanics of distributed fault and block rotation. In: (C. Kissel and C. Laj, Eds.), *Paleomagnetic Rotations and Continental Deformation,* Kluwer Academic Publ., 209-228. https://doi.org/10.1007/978-94-009-0869-7_14
100. Öztürk, S., 2018. Earthquake hazard potential in the Eastern Anatolian region of Turkey: seismotectonic b and Dc-values and precursory quiescence Z-value. *Front. Earth Sci*., **12**(1), 215-236. https://doi.org/10.1007/s11707-017-0642-3
101. Pechersky, D.M., Lyubushin, A.A. and Sharonova, Z.V., 2010. On the synchronism in the events within the core and on the surface of the earth: the changes in the organic world and in the polarity of the geomagnetic field in the Phanerozoic. *Izvestiya, Physics of the Solid Earth*, **46**, 613-623. https://doi.org/10.1134/S1069351310070050
102. Reilinger, R. E., McClusky, S., Vernant, P., Lawrence, S., Ergintav, S., Cakmak, R., Ozener, H., Kadirov, F., Guliyev, I. et al., 2006. GPS constraints on continental deformation in the Africa-Arabia-Eurasia continental

collision zone and implications for the dynamics of plate interactions. *Jour. of Geophysical Research*, **BO5411**, 1–26. https://doi.org/10.1029/2005JB004051

103. Ricard, Y., Vigny, C. and Froidevaux, C., 1989. Mantle heterogeneities, geoid, and plate motion: a Monte Carlo inversion. *Jour. of Geophysical Research*, **94** (B10), 13,739-13,754. https://doi.org/10.1029/JB094iB10p13739
104. Richards, M.A. and Hager, B.H., 1984. Geoid anomalies in a dynamic Earth. *Jour. of Geophysical Research*, **B 89**, 5987–6002. https://doi.org/10.1029/JB089iB07p05987
105. Rolland, Y., 2017. Caucasus collisional history: Review of data from East Anatolia to West Iran. *Gondwana Research*, **49**, 130-146. https://doi.org/10.1016/j.gr.2017.05.005
106. Rolland, Y., Hassig, M., Bosch, D., Bruguier, D., Melis, R., Galoyan, G., Topuz, G., Sahakyan, L., Avagyan, A. and Sosson, M., 2020. The East Anatolia–Lesser Caucasus ophiolite: An exceptional case of large-scale obduction, synthesis of data and numerical modelling. *Geosci. Front.*, **11**, 83-108. https://doi.org/10.1016/j.gsf.2018.12.009
107. Ron, H. and Baer, G., 1988. Paleomagnetism of Early Cretaceous rocks from southern Israel. *Israel Jour. of Earth Sci.*, **37**, 73-81.
108. Ron, H., Freund, R., Garfunkel, Z. and Nur, A., 1984. Block rotation by strike-slip faulting: structural and paleomagnetic evidence. *Jour. of Geophysical Research*, B **89**, 6256-6270. https://doi.org/10.1029/JB089IB07P06256
109. Sandwell, D.T. and Smith, W.H.F., 2009. Global marine gravity from retracked Geosat and ERS-1 altimetry: ridge segmentation versus spreading rate. *Jour. of Geophysical Research*, 114(B01411), 1–18. https://doi.org/10.1029/2008JB006008
110. Schmid, C., van der Lee, S., VanDecar, J.C., Engdahl, E.R. and Giardini, D., 2008. Three-dimensional S velocity of the mantle in the Africa-Eurasia plate boundary region from phase arrival times and regional waveforms. *Jour. of Geophys. Research*: Solid Earth **113**, Art. No. B03306. https://doi.org/10.1029/2005JB004193
111. Skobelin, E.A., Sharapov, I.P. and Bugayov, A.F., 1990. Deliberations of state and ways of perestroika in geology (Has plate tectonics resulted in a revolution in geology?). In: *Critical Aspects of the Plate Tectonics Theory*. Theophrastus Publ., Athens, Greece, Vol. **1**, 17-37.
112. Segev, A., 2000. Synchronous magmatic cycles during the fragmentation of Gondwana: Radiometric ages from the Levant and other provinces. *Tectonophysics*, **325**(3-4), 257-277. https://doi.org/10.1016/S0040-1951(00)00122-0
113. Segev, A., 2009. $^{40}Ar/^{39}Ar$ and K-Ar geochronology of Berriasian-Hauteririan and Cenomanian tectomagmatic events in northern Israel: implications for regional stratigraphy. *Cretaceous Research*, **30**, 818-828. https://doi.org/10.1016/j.cretres.2009.01.003
114. Segev, A. and Lang, B., 2002. 40Ar/39Ar dating of Valanginian top Tayasir Volcanics in the Mount Hermon area, northern Israel. Israel Geological Survey, *Current Research*, **13**, 100-104.
115. Segev, A. and Sass, E., 2009. The geology of the Carmel region, Albian-Turonian volcano-sedimentary cycles on the northwestern edge of the Arabian platform. *Rep. of the Israel Geol. Soc.*, Jerusalem, 1-77.
116. Segev, A., Weissbrod, T. and Lang, B., 2005. $^{40}Ar/^{39}Ar$ dating of the Aptian-Albian igneous rocks in Makhtesh Ramon (Negev, Israel) and its stratigraphic implications. *Cretaceous Research*, **26**, 633-656. https://doi.org/10.1016/j.cretres.2005.03.003
117. Şengör, A.M.C., Tüysüz, O., İmren, C., Sakınç, M., Eyidoğan, H., Görür, N., Le Pichon, X. and Rangin, C., 2005. The North Anatolian Fault: A New Look. *Annu. Rev. Earth Planet. Sci.*, **33**, 37-112. https://doi.org/10.1146/annurev.earth.32.101802.120415
118. Sharkov, E.V. and Khanna, S., 1987. Evolution of the upper mantle material in regions of intraplate magmatism: Case study of western Syria. *Doklady Acad. Sci. SSSR*, **297**, 684-686.
119. Shaliv, G., 1991. Stages in the tectonics and volcanic history of the Neogene basin in the Lower Galilee and the valleys. PhD Thesis, Hebrew Univ., Jerusalem (in Hebrew, summary in English).
120. Sharon, M., Sagy, A., Kurzon, I., Marco, S. and Rosensaft, M., 2020. Assessment of seismic sources and capable faults through hierarchic tectonic criteria: implications for seismic hazard in the Levant. *Nat. Hazards Earth Syst. Sci.*, **20**, 125-148. https://doi.org/10.5194/nhess-20-125-2020
121. Shimron, A.E., 1998. Tectonic evolution of the southern Mount Hermon. *Report Geol. Surv Israel Rep.* GSI/10/98.
122. Shimron, A.E. and Lang, B., 1989. New geological data and K-Ar geochronology of the magmatic rocks on the southeast flanks of Mount Hermon. *Geol. Surv. Israel Rep.* GSI/41/88.
123. Shimron, A.E. and Peltz, S., 1993. Early Cretaceous pyroclastic volcanism on the Hermon Range. *Geol. Surv. Israel Bull.*, **84**, p. 43.
124. Smit, J., Brun, J.-P., Cloetingh, S. and Z. Ben-Avraham, 2010. The rift-like structure and asymmetry of the Dead Sea Fault. *Earth Planet. Sci. Lett.*, **290**, 74-82. https://doi.org/10.1016/j.epsl.2009.11.060
125. Sneh, A., Bartov, Y. and Rozensaft, M., 1998. Geological Map of Israel, Scale 1:200,000. *Geol. Surv. of Israel*, Min. of Nation. Infrastructure, Jerusalem.

126. Stampfli, G.M., Hochard, C., Verard, C., Wilhem, C. and von Raumer, J., 2013. The formation of Pangea. *Tectonophysics*, **593**, 1-19. https://doi.org/10.1016/j.tecto.2013.02.037
127. Stein, R.S., Barka, A. and Dieterich, J.D., 1997. Progressive failure on the North Anatolian fault since 1939 by earthquake stress triggering. *Geoph. Jour. International*, **128**, 594-604. https://doi.org/10.1111/j.1365-246X.1997.tb05321.x
128. Stern, R.J. and Johnson, P.R., 2010. Continental lithosphere of the Arabian Plate: A geologic, petrologic, and geophysical synthesis. *Earth-Sci. Rev.*, **101**, 29-67. https://doi.org/10.1016/j.earscirev.2010.01.002
129. Su, W.-J., Woodward, R.L. and Dziewonski, A.M., 1994. Degree-12 model of shear velocity heterogeneity in the mantle. *Jour. of Geophys. Research*, Solid Earth, **99**, 4945-4980. https://doi.org/10.1029/93JB03408
130. Tatar, O., Piper, J.D.A., Gürsoy, H., Heimann, A. and Koşbulut, F., 2004. Neotectonic deformation in the transition zone between the Dead Sea Transform and the East Anatolian Fault Zone, Southern Turkey: a palaeomagnetic study of the Karasu Rift Volcanism. *Tectonophysics*, **385**, 17-43. https://doi.org/10.1016/j.tecto.2004.04.005
131. Tauxe, L., 2002. *Paleomagnetic Principles and Practice*. Kluwer Acad. Publishers, N.Y. – Boston – Dordrecht, 299 p.
132. Taylor, R.N. and Nesbitt, R.W., 1988. Light rare-earth enrichment of supra subduction-zone mantle: Evidence from the Troodos ophiolite, Cyprus. *Geology*, **16**, 448-451. https://doi.org/10.1130/0091-7613(1988)016<0448:LREEOS>2.3.CO;2
133. Telford, W.M., Geldart, L.R. and Sheriff, R.E., 1991. *Applied Geophysics*. Cambridge Univ. Press, Cambridge, 760 p.
134. Trubitsyn, V.P., 2010. The nature of the boundary between the upper and the lower mantle and its influence on convection. *Izvestiya, Phys. of the Solid Earth*, **46**, 461-476. https://doi.org/10.1134/S1069351310060017
135. Trubitsyn, V.P., 2012. Propagation of oceanic plates through the boundary between the upper and lower mantle. *Doklady Earth Sci.*, **446**, 1220-1222. https://doi.org/10.1134/S1069351308030014
136. Tselentis, G.-A. and Drakopoulos, J., 1990. Stress Transfer and Nonlinear Stress Accumulation at the North Anatolian Fault, Turkey. *PAGEOPH*, **132**, No. 4, 699-710. https://doi.org/10.1007/BF00876814
137. Uzel, B., Langereis, C. G., Kaymakci, N., Sozbilir, H., Ozkaymak, C. and Ozkaptan, M., 2015. Paleomagnetic Evidence for an Inverse Rotation History of Western Anatolia during the Exhumation of Menderes Core Complex. *Earth and Planet. Sci. Lett.*, **414**, 108-125. https://doi.org/10.1016/j.epsl.2015.01.008
138. Yudalevich, Z.A., Fershtater, G.B. and Eyal, M., 2014. Magmatism of Makhtesh-Ramon: Geology, geochemistry, petrogenesis (Conservation area Har Ha-Negev, Israel). *Lithosphere*, No. 3, 70-92 (in Russian).
139. Yudalevich, Z. and Vapnik, E., 2018. Xenocrysts and megacrysts of alkali-olivine-basalt-basanite-nephelinite association of Makhtesh Ramon (Israel): Interaction with transporting magmas and morphological adjustment. *Lithosphere*, **18**, No. 5, 70-92 (in Russian).
140. Van der Hilst, R.D., Widiyantoro, S. and Engdahl, E.R., 1997. Evidence for deep mantle circulation from global tomography. *Nature*, **386**, 578-584. https://doi.org/10.1038/386578a0
141. van der Meer, D.G., van Hinsbergen, D.J.J. and Spakman, W., 2018. Atlas of the underworld: Slab remnants in the mantle, their sinking history, and a new outlook on lower mantle viscosity. *Tectonophysics*, **723**, 309-448. https://doi.org/10.1016/j.tecto.2017.10.004
142. Vapnik, Y., Sharygin, V., Samoilov, V. and Yudalevich, Z., 2007. The petrogenesis of basic and ultrabasic alkaline rocks of Western Makhtesh Ramon, Israel: melt and fluid inclusion study. *Int. Jour. Earth Sci.* (Geol. Rundsh.), **96**, 663-684. https://doi.org/10.1007/s00531-006-0131-5
143. Véronnet, A., 1912. Rotation de l'Ellipsoide Hétérogène et Figure Exacte de la Terre. *J. Math. Pures et Appl.*, **8**, Ser. 6, 331–463.
144. Wen, L. and Helmberger, D.V., 1998. Ultra-low velocity zones near the core-mantle boundary from broadband PKP precursors. *Science*, **279**, 1701-1703. https://doi.org/10.1126/science.279.5357.17
145. Wilson, M., Shimron, A.E., Rosenbaum, J.M., Preston, J., 2000. Early Cretaceous magmatism of Mount Hermon, Northern Israel. *Contrib. to Mineralogy and Petrology*, **139**, No. 1, 54-67. https://doi.org/10.1007/s004100050573
146. Zak, I., 1968. Geological Map of Israel (1:20,000). Makhtesh Ramon, Har Gevanim. Israel Geol. Survey.
147. *Zilberman*, E. and *Avni*, Y., *2004a*. The geological map of Israel, 1:50,000. Sheet 21-I, Har Hamran. Israel Geol. Surv., Jerusalem.
148. Zilberman, E. and Avni, Y., 2004b. The geological map of Israel, 1: 50,000. Sheet 21-II: Mizpe Ramon. Israel Geol. Surv., Jerusalem.